

# MULTISCALE SCATTERED DATA ANALYSIS IN SAMPLET COORDINATES

SARA AVESANI, RÜDIGER KEMPF, MICHAEL MULTERER, AND HOLGER WENDLAND

**ABSTRACT.** We study multiscale scattered data interpolation schemes for globally supported radial basis functions with focus on the Matérn class. The multiscale approximation is constructed through a sequence of residual corrections, where radial basis functions with different lengthscale parameters are combined to capture varying levels of detail. We prove that the condition numbers of the diagonal blocks of the corresponding multiscale system remain bounded independently of the particular level, allowing us to use an iterative solver with a bounded number of iterations for the numerical solution. Employing an appropriate diagonal scaling, the multiscale system becomes well conditioned. We exploit this fact to derive a general error estimate bounding the consistency error issuing from a numerical approximation of the multiscale system. To apply the multiscale approach to large data sets, we suggest to represent each level of the multiscale system in samplet coordinates. Samplets are localized, discrete signed measures exhibiting vanishing moments and allow for the sparse approximation of generalized Vandermonde matrices issuing from a vast class of radial basis functions. Given a quasi-uniform set of  $N$  data sites, and local approximation spaces with exponentially decreasing dimension, the samplet compressed multiscale system can be assembled with cost  $\mathcal{O}(N \log^2 N)$ . The overall cost of the proposed approach is  $\mathcal{O}(N \log^2 N)$ . The theoretical findings are accompanied by extensive numerical studies in two and three spatial dimensions.

## 1. INTRODUCTION

Interpolation using radial basis functions (RBFs) is a widely recognized technique for fitting functions based on scattered data in  $\mathbb{R}^d$ , see [17, 20, 21] for some surveys. RBF interpolation allows for the construction of approximation spaces in arbitrary dimensions and with varying levels of smoothness. These spaces are well known to provide high-quality approximations, see [18, 37]. Even so, the computation of an RBF interpolant usually entails a significant computational cost and the corresponding linear system is typically ill-conditioned. Even worse, as the convergence order increases, the associated problems become successively ill-conditioned. Moreover, using globally supported RBFs in interpolation leads to densely populated matrices, making the problem computationally infeasible for larger datasets. To address the latter, techniques such as interpolation using compactly supported RBFs have been developed [27, 36]. Unfortunately, even interpolation with these RBFs either becomes computationally too expensive, if unscaled kernels are used, or does not even lead to convergence, if the support is scaled proportional to the fill-distance. Motivated by balancing this trade-off principle, the works [4, 6, 15, 29], among many others, leverage the idea of a multiscale method where approximations on different scales are computed in a residual correction scheme. To date, the most general convergence theorems for multiscale interpolation using positive definite, compactly supported RBFs have been developed in [29]. The advantage of the multiscale method is that the condition numbers of the resulting linear systems at each level remain independent of the particular level.

An effective approach to address the computational challenges of large datasets is the greedy kernel method [33]. The greedy kernel method systematically selects a representative subset of the data to construct a sparse approximation. An alternative strategy involves deep kernel methods [3, 23, 32, 34]. These methods leverage deep neural networks to learn adaptive feature representations, thereby constructing kernels that are tuned to the intrinsic structure of medium to high-dimensional data. Further, kernel multigrid methods [7, 13, 35] have been developed for the efficient numerical solution of partial differential equations on complex domains such as manifolds or point cloud

surfaces. These techniques use specialized kernels, such as polyharmonic or homogeneous kernels, along with localized Lagrange bases.

In this article, we study the RBF interpolation problem using globally supported RBFs. We address the challenge of dealing with densely-populated interpolation matrices by employing *samplelet compression*, a technique introduced in [9]. Samplelets are discrete signed measures constructed such that all polynomials up to a certain degree vanish. This vanishing moment property allows for the compression of generalized Vandermonde matrices issuing from *asymptotically smooth* RBFs, i.e., they behave like smooth functions apart from zero. Hence, in samplelet coordinates, the resulting interpolation matrices become quasi-sparse, which means that they can be compressed such that only a sparse matrix remains. Furthermore, samplelets allow for a respective sparse matrix algebra, see [11], and provide a meaningful interpretation of sparsity constraints for scattered data, see [2]. Unlike approaches that rely on the specific kernel, samplelets can be applied to a broad class of positive definite kernels.

However, as the samplelet transform of a given generalized Vandermonde matrix is an isometry up to the compression error, it does not alleviate the ill-conditioning. Therefore, to mitigate issues related to ill-conditioning, we adopt a multiscale interpolation approach that exploits scaled versions of the same RBF, which, in our case, remains globally supported. Especially, we extend the results from [29] for compactly supported RBFs to the class of Matérn kernels. As a consequence, the diagonally scaled multiscale system becomes well conditioned. We exploit this fact to derive a general error estimate bounding the consistency error issuing from a numerical approximation of the multiscale system. The theoretical results are corroborated by extensive numerical studies in two and three spatial dimensions.

The remainder of this article is organized as follows. In Section 2, we revisit the classical multiscale interpolation algorithm, detailing the relevant subspaces and the class of radial basis functions considered in this work. In Section 3 we carry over a known result for compactly supported functions to globally supported RBFs: The condition number of the generalized Vandermonde matrix can be bounded uniformly in the number of sites, if an appropriate scaling is applied. Section 4 derives a general approximation error estimate for the case that the block matrix in the multiscale system is numerically approximated. Section 5 provides a brief introduction of samplelets, with a focus on the key properties of the basis transformation and compression. In Section 6, we present the multiscale interpolation algorithm in the samplelet basis and provide error and cost estimates. Finally, in Section 7, we provide numerical tests in both two and three spatial dimensions. Concluding remarks are stated in Section 8.

Throughout this article, to avoid the excessive use of generic constants, we use the notation  $A \sim B$  to indicate that there exists constants  $\underline{c}, \bar{c} > 0$  independent of  $A, B$ , and any quantities they may depend on, such that  $\underline{c}A \leq B \leq \bar{c}A$ . In addition  $C > 0$  will always denote a generic constant, whose value can change depending on the context.

## 2. CLASSICAL MULTISCALE METHOD

Let  $\Omega \subseteq \mathbb{R}^d$  be a domain and  $X = \{\mathbf{x}_1, \dots, \mathbf{x}_N\} \subseteq \Omega$  be a set of data sites with cardinality  $N := \#X$ . Moreover, let  $f \in C(\Omega)$  be the function generating the data values  $f_1, \dots, f_N$  corresponding to  $\mathbf{x}_1, \dots, \mathbf{x}_N$ . Associated to the set of data sites  $X$ , there are two measures, namely the *fill-distance* of  $X$  in  $\Omega$  and the *separation radius* of  $X$ , i.e.,

$$h_{X,\Omega} := \sup_{\mathbf{x} \in \Omega} \min_{\mathbf{x} \in X} \|\mathbf{x} - \mathbf{x}_j\|_2, \quad q_X := \frac{1}{2} \min_{j \neq k} \|\mathbf{x}_j - \mathbf{x}_k\|_2.$$

We call  $X$  *quasi-uniform* if there exists a constant  $c_{\text{qu}} > 0$  such that  $q_X \leq h_{X,\Omega} \leq c_{\text{qu}} q_X$ .

Our goal is to interpolate or approximate the target function by means of RBFs only relying on the given data  $(\mathbf{x}_1, f_1), \dots, (\mathbf{x}_N, f_N)$ . A function  $\Phi: \mathbb{R}^d \rightarrow \mathbb{R}$  is said to be *radial*, if and only if there exists a univariate function  $\phi: [0, \infty) \rightarrow \mathbb{R}$  such that  $\Phi(\mathbf{x}) = \phi(\|\mathbf{x}\|_2)$ . The radial function  $\Phi$  is *strictly positive definite*, if and only if there holds for any choice of distinct points  $\boldsymbol{\xi}_1, \dots, \boldsymbol{\xi}_n, n \in \mathbb{N}$ ,

that  $\boldsymbol{\alpha}^\top [\Phi(\boldsymbol{\xi}_i - \boldsymbol{\xi}_j)]_{i,j} \boldsymbol{\alpha} > 0$  for all  $\boldsymbol{\alpha} \in \mathbb{R}^n \setminus \{\mathbf{0}\}$ . In this case, the kernel  $K(\mathbf{x}_i, \mathbf{x}_j) := \Phi(\mathbf{x}_i - \mathbf{x}_j)$  is the reproducing kernel of a uniquely determined reproducing kernel Hilbert space, its *native space*, that we denote by  $(\mathcal{N}_\Phi, \langle \cdot, \cdot \rangle_{\mathcal{N}_\Phi})$ . In this context, we will use the function  $\Phi$  and its associated kernel  $K$  synonymously. A popular class of strictly positive RBFs are the *Matérn kernels* or *Sobolev splines*  $\Phi_\theta: \mathbb{R}^d \rightarrow \mathbb{R}$ , dependent on the hyper-parameter  $\theta > d/2$ , that steers the smoothness of the kernel. These kernels are defined via the radial function

$$(1) \quad \phi_\theta(r) = \frac{2^{1-\theta+d/2}}{\Gamma(\theta-d/2)} r^{\theta-d/2} K_{\theta-d/2}(r), \quad r \geq 0,$$

where  $\Gamma$  is the Riemann gamma function and  $K_\nu$  is the modified Bessel function of the second kind of order  $\nu$ , see [19] for example. It is well-known that the Fourier transform of this radial function satisfies

$$(2) \quad \mathcal{F}\Phi(\boldsymbol{\omega}) = (1 + \|\boldsymbol{\omega}\|_2^2)^{-\theta}, \quad \boldsymbol{\omega} \in \mathbb{R}^d,$$

and that, in turn, the native space of the corresponding Matérn kernel is norm-equivalent to the Sobolev space  $H^\theta(\mathbb{R}^d)$ , see [28, Corollary 10.13] for example.

In this *instationary setting*, meaning that the length-scale of the kernel is not coupled to the fill-distance, it is known that the interpolant  $s \in \mathcal{S} := \text{span}\{\Phi(\cdot - \mathbf{x}) : \mathbf{x} \in X\} \subset \mathcal{N}_\Phi$  converges towards the function  $f$  as  $h_{X,\Omega} \rightarrow 0$ . However, this improved approximation comes with higher and higher numerical cost for the iterative solution due to the ill-conditioning of the associated generalized Vandermonde matrix. To alleviate this cost, we can rescale the kernel, i.e., we introduce the parameter  $\delta > 0$  and define

$$(3) \quad \Phi_\delta := \delta^{-d} \Phi\left(\frac{\cdot}{\delta}\right).$$

In this *stationary setting*, we couple  $\delta$  proportional to  $h_{X,\Omega}$ , i.e., there is a *coupling parameter*  $\eta > 0$  such that

$$(4) \quad \delta = \eta h_{X,\Omega}.$$

In this case, we can control the numerical costs to compute the interpolant but cannot expect convergence. This is known as the *trade-off principle*.

The idea of the multiscale method is now to introduce a hierarchy

$$(5) \quad X_1, X_2, \dots, X_L = X,$$

where we refer to the subscript of  $X_\ell$  as level with cardinalities  $N_\ell := \#X_\ell$  and fill-distances  $h_\ell := h_{X_\ell,\Omega}$ . Although in many applications the sets will be nested, for the multiscale method itself, this is not necessary. We assume that the cardinalities of the sets  $X_\ell$  are increasing with the level, i.e.,  $N_\ell \leq N_{\ell+1}$  or, in other words,  $h_\ell \geq h_{\ell+1}$ . We quantify this relation in Theorem 2.1. In what follows, we consider the stationary setting at each level  $\ell$ . This yields level-dependent parameters  $\delta_\ell > 0$  and level-dependently rescaled kernels  $K_\ell$  given by

$$(6) \quad K_\ell(\mathbf{x}, \mathbf{y}) := \Phi_\ell(\mathbf{x} - \mathbf{y}) = \delta_\ell^{-d} \Phi\left(\frac{\mathbf{x} - \mathbf{y}}{\delta_\ell}\right), \quad \mathbf{x}, \mathbf{y} \in \mathbb{R}^d, \quad \ell = 1, \dots, L.$$

Each set  $X_\ell$  in the multiscale hierarchy (5), together with the respective kernel, gives rise to a subspace

$$(7) \quad \mathcal{S}_\ell := \text{span}\{\Phi_\ell(\cdot - \mathbf{x}) : \mathbf{x} \in X_\ell\} \subset \mathcal{N}_{\Phi_\ell},$$

called the *local approximation space*.

Now, given the multiscale sequence  $X_1, \dots, X_L$ , we seek an approximation in terms of successive residual corrections. To this end, we introduce functions  $w_\ell$  of the form

$$(8) \quad w_\ell = \sum_{i=1}^{N_\ell} c_{\ell,i} \Phi_\ell(\cdot - \mathbf{x}_i) \in \mathcal{S}_\ell.$$

The coefficients  $c_{\ell,i}$  are determined from decomposing the approximation problem by a telescoping sum according to

$$\begin{aligned} s_1|_{X_1} &=: w_1|_{X_1} = f|_{X_1}, \\ w_2|_{X_2} &= (f - w_1)|_{X_2}, \\ &\vdots \\ w_L|_{X_L} &= \left( f - \sum_{\ell=1}^{L-1} w_\ell \right)|_{X_L}. \end{aligned}$$

This means that, at level  $\ell$ , we compute the interpolant to the residual at level  $\ell - 1$ , i.e.,

$$(9) \quad f - (w_1 + \dots + w_{\ell-1})$$

in the space  $\mathcal{S}_\ell$ . From this, we obtain the multiscale decomposition  $s_L := (w_1 + \dots + w_L) \in \cup_{\ell=1}^L \mathcal{S}_\ell$  which matches  $f$  at each of the data sites in  $X$ , i.e.,  $s_L|_X = f|_X$ .

In practice, the multiscale approximation process begins with a small set of points, where the approximation problem (8) is solved. Next, the error function (9) is computed, and finally, the latter is approximated at a finer scale. The coefficients of the residual correction at level  $\ell$  can be computed by solving

$$\mathbf{K}_{\ell,\ell} \mathbf{c}_\ell = \mathbf{f}_\ell - \sum_{\ell'=1}^{\ell-1} \mathbf{K}_{\ell,\ell'} \mathbf{c}_{\ell'}$$

with the *generalized Vandermonde matrices*  $\mathbf{K}_{\ell,\ell'} := [\Phi_{\ell'}(\mathbf{x}_i^{(\ell)} - \mathbf{x}_j^{(\ell')})]_{i,j} \in \mathbb{R}^{N_\ell \times N_{\ell'}}$  and the vectors  $\mathbf{f}_\ell := \mathbf{f}|_{X_\ell} \in \mathbb{R}^{N_\ell}$ ,  $\mathbf{c}_\ell := [c_{\ell,i}]_i \in \mathbb{R}^{N_\ell}$ . Consequently, the coefficient vectors  $\mathbf{c}_1, \dots, \mathbf{c}_L$  are obtained by solving the block lower triangular system

$$(10) \quad \mathcal{K} \mathbf{c} := \begin{bmatrix} \mathbf{K}_{1,1} & & \\ \mathbf{K}_{2,1} & \mathbf{K}_{2,2} & \\ \vdots & \vdots & \ddots \\ \mathbf{K}_{L,1} & \mathbf{K}_{L,2} & \dots & \mathbf{K}_{L,L} \end{bmatrix} \begin{bmatrix} \mathbf{c}_1 \\ \mathbf{c}_2 \\ \vdots \\ \mathbf{c}_L \end{bmatrix} = \begin{bmatrix} \mathbf{f}_1 \\ \mathbf{f}_2 \\ \vdots \\ \mathbf{f}_L \end{bmatrix} =: \mathbf{f}.$$

The resulting block matrix  $\mathcal{K}$  is in general a densely-populated lower triangular matrix as a result of the choice of globally supported RBFs for the approximation at each level. There holds the following convergence result, see, e.g., [29, 30].

**Theorem 2.1.** *Let  $\Omega \subseteq \mathbb{R}^d$  be a bounded domain with Lipschitz boundary. Let  $X_1, X_2, \dots$  be a sequence of point sets in  $\Omega$  with fill-distances  $h_1, h_2, \dots$  satisfying*

$$(11) \quad c\mu h_\ell \leq h_{\ell+1} \leq \mu h_\ell$$

*for  $\ell = 1, 2, \dots$  with fixed  $\mu \in (0, 1)$ ,  $c \in (0, 1]$  and  $h_1$  sufficiently small. Further, let  $\Phi: \mathbb{R}^d \rightarrow \mathbb{R}$  be a reproducing kernel for  $H^\theta(\mathbb{R}^d)$ , i.e., its Fourier transform satisfies  $\mathcal{F}\Phi(\boldsymbol{\omega}) \sim (1 + \|\boldsymbol{\omega}\|_2^2)^{-\theta}$ ,  $\boldsymbol{\omega} \in \mathbb{R}^d$  and let  $\Phi_\ell$  be the rescaled kernel as in (3) with scale factor  $\delta_\ell = \eta h_\ell$ ,  $\eta > 1$ . Let  $f \in H^\theta(\Omega)$ . Then there exist constants  $C$  and  $C_1 > 0$  such that*

$$\|f - s_L\|_{L_2(\Omega)} \leq C(C_1\mu^\theta + C_1\eta^{-\theta})^L \|f\|_{H^\theta(\Omega)}.$$

### 3. CONDITION NUMBER BOUND FOR GENERALIZED VANDERMONDE MATRICES

We now show that the condition number of the generalized Vandermonde matrices  $\mathbf{K}_{\ell,\ell}$ ,  $\ell = 1, \dots, L$ , of the scaled kernel can be bounded by a constant, independently of the level  $\ell$ . A similar result in the context of the multiscale method for compactly supported RBFs has been derived in [26] using techniques of [22, 24]. We will reuse these techniques, with appropriate modifications. Furthermore, for a lighter notation, we will drop the subscripts  $\ell$  in this section.

It goes without saying that, such a bound can not be established for general sets of data sites  $X$ . Hence, for this section, we assume that  $X$  is quasi-uniform and the parameters of the multilevel method are chosen as in Theorem 2.1.

We remark that the algebraic decay of the Fourier transform of the Matérn kernel (2) immediately yields for the scaled RBF  $\Phi_\delta$  that  $\mathcal{F}\Phi_\delta(\boldsymbol{\omega}) = (1 + \delta^2 \|\boldsymbol{\omega}\|_2^2)^{-\theta}$ ,  $\boldsymbol{\omega} \in \mathbb{R}^d$ . We will bound the smallest and largest eigenvalue of the matrix  $\mathbf{K}$  separately. We follow the ideas of [22, 24, 26].

**Theorem 3.1.** *Let  $\Omega \subseteq \mathbb{R}^d$  be a bounded domain and  $X \subseteq \Omega$  be a quasi-uniform set of data sites with fill-distance  $h_{X,\Omega}$  and separation radius  $q_X$ . Let  $\Phi$  be the Matérn kernel with smoothness parameter  $\theta$ . Let  $\Phi_\delta = \delta^{-d}\Phi(\cdot/\delta)$  be the rescaled kernel where  $\delta = \eta h_{X,\Omega}$  with overlap parameter  $\eta > 1$ . Then there exists a constant  $C = C(\Phi, d)$  such that the smallest eigenvalue  $\lambda_{\min}$  of  $\mathbf{K} = [\Phi_\delta(\mathbf{x}_i - \mathbf{x}_j)]_{i,j}$  satisfies  $\lambda_{\min}(\mathbf{K}) \geq C(\eta c_{\text{qu}})^{d-2\theta} \delta^{-d}$ , while the largest eigenvalue of  $\mathbf{K}$  can be bounded from above by  $\lambda_{\max}(\mathbf{K}) \leq \tilde{C} \delta^{-d}$ , with a constant  $\tilde{C} = C(\Phi, d, \eta, c_{\text{qu}})$ .*

*Proof.* We set

$$\widetilde{\mathbf{K}} = \delta^d \mathbf{K} = \left[ \Phi\left(\frac{\mathbf{x}_i - \mathbf{x}_j}{\delta}\right) \right]_{i,j}.$$

The lower bound immediately follows from [26, Proof of Proposition 3.4]. Hence, we only prove the upper bound for  $\lambda_{\max}(\mathbf{K})$ . To this end, we apply Gershgorin's circle theorem, see, e.g., [31, Theorem 5.1] to  $\widetilde{\mathbf{K}}$ . Since the diagonal elements of this matrix are  $\Phi(\mathbf{0})$ , independently of the row  $i$ , we can, without loss of generality, set  $i = 1$  and  $\mathbf{x}_1 = \mathbf{0}$ . We have

$$(12) \quad |\lambda - \Phi(\mathbf{0})| \leq \sum_{k=2}^N \left| \Phi\left(\frac{\mathbf{0} - \mathbf{x}_k}{\delta}\right) \right| = \sum_{k=2}^N \left| \Phi\left(\frac{\mathbf{x}_k}{\delta}\right) \right|.$$

To bound the right hand side of this estimate, we introduce the annuli  $E_n$  given by

$$E_n = \{\mathbf{x} \in \mathbb{R}^d : nq_X \leq \|\mathbf{x}\|_2 < (n+1)q_X\}.$$

Each  $\mathbf{x}_k$  is contained in exactly one  $E_n$  and we can estimate

$$\#\{\mathbf{x}_k \in E_n\} \leq 3^d n^{d-1},$$

see, e.g., [28, Proof of Theorem 12.3]. Inserting this into (12) yields

$$(13) \quad \begin{aligned} |\lambda_{\max}(\widetilde{\mathbf{K}}) - \Phi(\mathbf{0})| &\leq \sum_{k=2}^N \left| \Phi\left(\frac{\mathbf{x}_k}{\delta}\right) \right| \leq \sum_{n=1}^{\infty} \sum_{\mathbf{x}_k \in E_n} \left| \Phi\left(\frac{\mathbf{x}_k}{\delta}\right) \right| \\ &\leq \sum_{n=1}^{\infty} \#\{\mathbf{x}_k \in E_n\} \sup_{\mathbf{x} \in E_n} \left| \Phi\left(\frac{\mathbf{x}}{\delta}\right) \right|. \end{aligned}$$

Next, we bound  $\sup_{\mathbf{x} \in E_n} |\Phi(\mathbf{x}/\delta)|$ . We use the specific form of  $\Phi$ , cp. (1), and the fact that the function  $r \mapsto r^\beta K_\beta(r)$  is non-increasing on  $(0, \infty)$  for any  $\beta \in \mathbb{R}$ , see [28, Corollary 5.12]. This yields

$$\begin{aligned} \frac{\Gamma(\theta - \frac{d}{2})}{2^{1-\theta+\frac{d}{2}}} \sup_{\mathbf{x} \in E_n} \left| \Phi\left(\frac{\mathbf{x}}{\delta}\right) \right| &= \sup_{\mathbf{x} \in E_n} \left( \frac{\|\mathbf{x}\|_2}{\delta} \right)^{\theta - \frac{d}{2}} K_{\theta - \frac{d}{2}}\left(\frac{\|\mathbf{x}\|_2}{\delta}\right) \\ &\leq \left( \frac{nq_X}{\delta} \right)^{\theta - \frac{d}{2}} K_{\theta - \frac{d}{2}}\left(\frac{nq_X}{\delta}\right) \\ &\leq \left( \frac{nq_X}{\delta} \right)^{\theta - \frac{d}{2}} \sqrt{2\pi} \left( \frac{\delta}{nq_X} \right)^{\frac{1}{2}} \exp\left(-\frac{nq_X}{\delta}\right) \exp\left(\left(\theta - \frac{d}{2}\right)^2 \frac{2\delta}{2nq_X}\right), \end{aligned}$$

where we used the asymptotic behavior [28, Lemma 5.13] of the modified Bessel function to arrive at the last inequality. Inserting this into (13), using the quasi-uniformity of  $X$  and the coupling of

$\delta$  to  $h_{X,\Omega}$ , as in Theorem 2.1, yields

$$\begin{aligned} |\lambda_{\max}(\widetilde{\mathbf{K}}) - \Phi(\mathbf{0})| &\leq \sum_{n=1}^{\infty} \#\{\mathbf{x}_k \in E_n\} \sup_{\mathbf{x} \in E_n} \left| \Phi\left(\frac{\mathbf{x}}{\delta}\right) \right| \\ &\leq \sum_{n=1}^{\infty} 3^d n^{d-1} \sqrt{2\pi} \eta^{\frac{d}{2}-\theta} (\eta c_{\text{qu}})^{\frac{1}{2}} n^{\theta-\frac{d}{2}-\frac{1}{2}} \exp\left(-\frac{n}{\eta} + \frac{(\theta-\frac{d}{2})^2 \eta c_{\text{qu}}}{n}\right) \\ &\leq \sqrt{2\pi} 3^d \eta^{\frac{d}{2}-\theta} (\eta c_{\text{qu}})^{\frac{1}{2}} \sum_{n=1}^{\infty} n^{\theta-\frac{d}{2}-\frac{3}{2}} \exp\left(-\frac{n}{\eta} + \frac{(\theta-\frac{d}{2})^2 \eta c_{\text{qu}}}{n}\right). \end{aligned}$$

Since the series on the right hand side of the estimate converges, this yields the claimed bound for  $\lambda_{\max}$ .  $\square$

The derived bounds on  $\lambda_{\min}$  and  $\lambda_{\max}$  lead to the boundedness of the condition number of the generalized Vandermonde matrices  $\mathbf{K}_{\ell,\ell}$  for  $\ell = 1, \dots, L$ , uniformly in the number of data sites and the scaling parameter. In addition, by a suitable diagonal scaling, also the lower triangular system in (10) becomes well conditioned. We have the following

**Corollary 3.2.** *For every  $\ell \in \mathbb{N}$  the condition number  $\text{cond}_2(\mathbf{K}_{\ell,\ell})$  is bounded independently of  $N_\ell$  and  $\delta_\ell$ . Furthermore, introducing the block diagonal scaling  $\mathcal{D} := \text{diag}(\delta_1^d \mathbf{I}, \dots, \delta_L^d \mathbf{I})$ , the diagonally scaled matrix  $\mathcal{D}^{1/2} \mathcal{K} \mathcal{D}^{1/2}$ , cp. (10) is well conditioned, i.e., the corresponding condition number satisfies  $\text{cond}_2(\mathcal{D}^{1/2} \mathcal{K} \mathcal{D}^{1/2}) \sim \text{cond}_F(\mathcal{D}^{1/2} \mathcal{K} \mathcal{D}^{1/2}) \sim 1$ .*

#### 4. NUMERICAL APPROXIMATION OF THE MULTISCALE SYSTEM

In this paragraph, we discuss the approximation error issuing from replacing the matrix  $\mathcal{K}$  of the multiscale system in (10) by an approximation  $\widehat{\mathcal{K}}$ .

As has been observed in Corollary 3.2, the multiscale system becomes well-conditioned by suitable diagonal scaling. For our analysis, we therefore consider the preconditioned matrix  $\mathcal{K}_{\text{pc}} := \mathcal{D}^{1/2} \mathcal{K} \mathcal{D}^{1/2}$  and its numerical approximation  $\widehat{\mathcal{K}}_{\text{pc}} := \mathcal{D}^{1/2} \widehat{\mathcal{K}} \mathcal{D}^{1/2}$ . We have the following standard perturbation result, see, e.g., [12].

**Lemma 4.1.** *Let  $\widehat{\mathcal{K}}$  be sufficiently close to  $\mathcal{K}$  and let  $\mathcal{K}_{\text{pc}} \mathbf{d} = \mathcal{D}^{1/2} \mathbf{f}$  and  $\widehat{\mathcal{K}}_{\text{pc}} \widehat{\mathbf{d}} = \mathcal{D}^{1/2} \mathbf{f}$ . Then there exists a constant  $C > 0$  such that the relative consistency error satisfies*

$$\frac{\|\mathbf{d} - \widehat{\mathbf{d}}\|_2}{\|\mathbf{d}\|_2} \leq C \frac{\|\mathcal{K}_{\text{pc}} - \widehat{\mathcal{K}}_{\text{pc}}\|_F}{\|\mathcal{K}_{\text{pc}}\|_F}.$$

*Proof.* The proof follows similarly to the proof of [12, Theorem 7.2]. There holds

$$\mathcal{K}_{\text{pc}}(\widehat{\mathbf{d}} - \mathbf{d}) = -(\widehat{\mathcal{K}}_{\text{pc}} - \mathcal{K}_{\text{pc}})\mathbf{d} + (\widehat{\mathcal{K}}_{\text{pc}} - \mathcal{K}_{\text{pc}})(\mathbf{d} - \widehat{\mathbf{d}})$$

Hence, by multiplying by  $\mathcal{K}_{\text{pc}}^{-1}$ , taking norms and exploiting the consistency of the Frobenius and the Euclidean norm, we obtain

$$\|\mathbf{d} - \widehat{\mathbf{d}}\|_2 \leq \|\mathcal{K}_{\text{pc}}^{-1}\|_F \|\widehat{\mathcal{K}}_{\text{pc}} - \mathcal{K}_{\text{pc}}\|_F \|\mathbf{d}\|_2 + \|\mathcal{K}_{\text{pc}}^{-1}\|_F \|\widehat{\mathcal{K}}_{\text{pc}} - \mathcal{K}_{\text{pc}}\|_F \|\mathbf{d} - \widehat{\mathbf{d}}\|_2.$$

Factoring out common terms and simplifying the expression then results in

$$\|\mathbf{d} - \widehat{\mathbf{d}}\|_2 \leq \frac{\|\mathcal{K}_{\text{pc}}^{-1}\|_F \|\widehat{\mathcal{K}}_{\text{pc}} - \mathcal{K}_{\text{pc}}\|_F}{1 - \|\mathcal{K}_{\text{pc}}^{-1}\|_F \|\widehat{\mathcal{K}}_{\text{pc}} - \mathcal{K}_{\text{pc}}\|_F} \|\mathbf{d}\|_2.$$

Dividing by  $\|\mathbf{d}\|_2$  and expanding the respective terms in the numerator and denominator by  $\|\mathcal{K}_{\text{pc}}\|_F$  finally gives

$$\frac{\|\mathbf{d} - \widehat{\mathbf{d}}\|_2}{\|\mathbf{d}\|_2} \leq \frac{\text{cond}_F(\mathcal{K}_{\text{pc}})}{1 - \text{cond}_F(\mathcal{K}_{\text{pc}}) \|\mathcal{K}_{\text{pc}} - \widehat{\mathcal{K}}_{\text{pc}}\|_F / \|\mathcal{K}_{\text{pc}}\|_F} \frac{\|\mathcal{K}_{\text{pc}} - \widehat{\mathcal{K}}_{\text{pc}}\|_F}{\|\mathcal{K}_{\text{pc}}\|_F}.$$

For a sufficiently small consistency error, we arrive at the claimed bound using Corollary 3.2.  $\square$

To connect the previous error estimate to the consistency error of the multiscale interpolant, we require the following technical lemma.

**Lemma 4.2.** *Consider any function  $v_\ell = \sum_{i=1}^{N_\ell} a_i \Phi_\ell(\cdot - \mathbf{x}_i^{(\ell)}) \in \mathcal{S}_\ell$ . Then, there holds*

$$\|v_\ell\|_{\mathcal{N}_{\Phi_\ell}} \sim \delta_\ell^{-d/2} \|\mathbf{a}\|_2 \quad \text{as well as} \quad \|v_\ell|X_\ell\|_{\ell^2} \sim \delta_\ell^{-d} \|\mathbf{a}\|_2,$$

where  $\mathbf{a} := [a_1, \dots, a_{N_\ell}]^\top$  is the coefficient vector of  $v_\ell$ .

*Proof.* By the reproducing property and due to  $\|\mathbf{K}_{\ell,\ell}\|_2 \sim \|\mathbf{K}_{\ell,\ell}^{-1}\|_2 \sim \delta_\ell^{-d}$ , we obtain

$$\|v_\ell\|_{\mathcal{N}_{\Phi_\ell}}^2 = \mathbf{v}^\top \mathbf{K}_{\ell,\ell} \mathbf{a} \sim \|\mathbf{K}_{\ell,\ell}\|_2 \|\mathbf{a}\|_2^2 \sim \delta_\ell^{-d} \|\mathbf{a}\|_2^2.$$

Taking square roots yields the first claim. Similarly, we observe

$$\|v_\ell|X_\ell\|_{\ell^2}^2 = \|\mathbf{K}_{\ell,\ell} \mathbf{a}\|_2^2 = \mathbf{a}^\top \mathbf{K}_{\ell,\ell}^2 \mathbf{a} \sim \delta_\ell^{-2d} \|\mathbf{a}\|_2^2$$

and the second claim is again obtained by taking square roots.  $\square$

Combining the previous two lemmata, we obtain a bound on the consistency error of the residual corrections.

**Theorem 4.3.** *Let  $w_\ell = \sum_{i=1}^{N_\ell} c_{\ell,i} \Phi_\ell(\cdot - \mathbf{x}_i) \in \mathcal{S}_\ell$  for  $\ell = 1, \dots, L$  denote the residual corrections obtained from the solution of  $\mathcal{K}\mathbf{c} = \mathbf{f}$ , see (10), and let  $\hat{w}_\ell = \sum_{i=1}^{N_\ell} \hat{c}_{\ell,i} \Phi_\ell(\cdot - \mathbf{x}_i) \in \mathcal{S}_\ell$  for  $\ell = 1, \dots, L$  be the residual corrections obtained from solving the perturbed system  $\hat{\mathcal{K}}\hat{\mathbf{c}} = \mathbf{f}$ . Then, there holds*

$$\frac{\sum_{\ell=1}^L \|w_\ell - \hat{w}_\ell\|_{\mathcal{N}_{\Phi_\ell}}^2}{\sum_{\ell=1}^L \|w_\ell\|_{\mathcal{N}_{\Phi_\ell}}^2} \leq C \frac{\|\mathcal{K}_{\text{pc}} - \hat{\mathcal{K}}_{\text{pc}}\|_F^2}{\|\mathcal{K}_{\text{pc}}\|_F^2}$$

for a constant  $C > 0$ .

*Proof.* Since the solutions to the original systems and their preconditioned versions are connected via  $\mathbf{d} = \mathcal{D}^{-1/2} \mathbf{c}$  and  $\hat{\mathbf{d}} = \mathcal{D}^{-1/2} \hat{\mathbf{c}}$ , respectively, the first equivalence in Lemma 4.2 yields

$$\|w_\ell - \hat{w}_\ell\|_{\mathcal{N}_{\Phi_\ell}}^2 \sim \delta_\ell^{-d} \|\mathbf{c}_\ell - \hat{\mathbf{c}}_\ell\|_2^2 = \|\mathbf{d}_\ell - \hat{\mathbf{d}}_\ell\|_2^2$$

as well as

$$\|w_\ell\|_{\mathcal{N}_{\Phi_\ell}}^2 \sim \delta_\ell^{-d} \|\mathbf{c}_\ell\|_2^2 = \|\mathbf{d}_\ell\|_2^2.$$

In view of  $\|\mathbf{d} - \hat{\mathbf{d}}\|_2^2 = \sum_{\ell=1}^L \|\mathbf{d}_\ell - \hat{\mathbf{d}}_\ell\|_2^2$  and  $\|\mathbf{d}\|_2^2 = \sum_{\ell=1}^L \|\mathbf{d}_\ell\|_2^2$ , we arrive at

$$\frac{\sum_{\ell=1}^L \|w_\ell - \hat{w}_\ell\|_{\mathcal{N}_{\Phi_\ell}}^2}{\sum_{\ell=1}^L \|w_\ell\|_{\mathcal{N}_{\Phi_\ell}}^2} \sim \frac{\|\mathbf{d} - \hat{\mathbf{d}}\|_2^2}{\|\mathbf{d}\|_2^2} \leq C \frac{\|\mathcal{K}_{\text{pc}} - \hat{\mathcal{K}}_{\text{pc}}\|_F^2}{\|\mathcal{K}_{\text{pc}}\|_F^2}$$

by employing Lemma 4.1. This completes the proof.  $\square$

To bound the numerical approximation error between  $s_L$  and  $\hat{s}_L := \hat{w}_1 + \dots + \hat{w}_L$ , we have the following result, which links this error to the approximation error of the residual corrections.

**Lemma 4.4.** *Under the conditions of Theorem 4.3, the approximation  $\hat{s}_L := \hat{w}_1 + \dots + \hat{w}_L$  to  $s_L$  satisfies the estimate*

$$\|s_L - \hat{s}_L\|_{L^2(\Omega)}^2 \leq CL \sum_{\ell=1}^L \|w_\ell - \hat{w}_\ell\|_{\mathcal{N}_{\Phi_\ell}}^2.$$

for some constant  $C > 0$ .

*Proof.* From the Cauchy–Schwarz inequality, it follows that

$$\|s_L - \hat{s}_L\|_{L^2(\Omega)}^2 = \left\| \sum_{\ell=1}^L (w_\ell - \hat{w}_\ell) \right\|_{L^2(\Omega)}^2 \leq L \sum_{\ell=1}^L \|w_\ell - \hat{w}_\ell\|_{L^2(\Omega)}^2.$$

Next, we consider the sampling inequality from [16, Theorem 3.5], i.e.,

$$\|u\|_{L^p} \leq C \left( h_{X,\Omega}^\theta \|u\|_{H^\theta(\Omega)} + h_{X,\Omega}^{d/p} \|u|X\|_{\ell^2} \right), \quad C > 0.$$

Letting  $p = 2$  and squaring the previous inequality results in

$$\|u\|_{L^2(\Omega)}^2 \leq 2C \left( h_{X,\Omega}^{2\theta} \|u\|_{H^\theta(\Omega)}^2 + h_{X,\Omega}^d \|u\|_{X\|_{\ell^2}}^2 \right).$$

Inserting this in the first inequality, we arrive at

$$\|s_L - \widehat{s}_L\|_{L^2(\Omega)}^2 \leq 2CL \sum_{\ell=1}^L \left( h_\ell^{2\theta} \|w_\ell - \widehat{w}_\ell\|_{H^\theta(\Omega)}^2 + h_\ell^d \|w_\ell - \widehat{w}_\ell\|_{X_\ell\|_{\ell^2}}^2 \right).$$

Next, we have from [29, Lemma 1] that

$$\|w_\ell - \widehat{w}_\ell\|_{H^\theta(\Omega)}^2 \leq C \delta_\ell^{-2\theta} \|w_\ell - \widehat{w}_\ell\|_{\mathcal{N}_{\Phi_\ell}}^2, \quad C > 0,$$

while the second equivalence in Lemma 4.2 amounts to

$$\|w_\ell - \widehat{w}_\ell\|_{X_\ell\|_{\ell^2}}^2 \sim \delta_\ell^{-2d} \|\mathbf{c}_\ell - \widehat{\mathbf{c}}_\ell\|_2^2 \sim \delta_\ell^{-d} \|w_\ell - \widehat{w}_\ell\|_{\mathcal{N}_{\Phi_\ell}}^2.$$

Inserting these two estimates in the previous one yields with  $\delta_\ell = \eta h_\ell$ , cp. (4), that

$$\|s_L - \widehat{s}_L\|_{L^2(\Omega)}^2 \leq CL \sum_{\ell=1}^L \left( \eta^{-2\theta} \|w_\ell - \widehat{w}_\ell\|_{\mathcal{N}_{\Phi_\ell}}^2 + \eta^{-d} \|w_\ell - \widehat{w}_\ell\|_{\mathcal{N}_{\Phi_\ell}}^2 \right),$$

for some constant  $C > 0$ , from which the claim is immediately obtained.  $\square$

Finally, we need a bound on the residual corrections by the right hand side  $f$ .

**Lemma 4.5.** *Under the conditions of Theorem 2.1, there exists a constant  $C > 0$  such that*

$$\sum_{\ell=1}^L \|w_\ell\|_{\mathcal{N}_{\Phi_\ell}}^2 \leq C \|f\|_{H^\theta(\Omega)}^2.$$

*Proof.* By construction, the residual correction  $w_\ell$  is the norm-minimal interpolant to the residual  $e_{\ell-1} := f - \sum_{m=1}^{\ell-1} w_m$ , for any  $1 \leq \ell \leq L$ , which implies

$$\|w_\ell\|_{\mathcal{N}_{\Phi_\ell}} \leq \|Ee_{\ell-1}\|_{\mathcal{N}_{\Phi_\ell}}$$

with the continuous extension operator  $E: H^\theta(\Omega) \rightarrow H^\theta(\mathbb{R}^d)$ ,  $\|Ef\|_{H^\theta(\mathbb{R}^d)} \leq C_E \|f\|_{H^\theta(\Omega)}$ . Now we can use the recursion estimate [29, Theorem 1] to obtain

$$\|Ee_{\ell-1}\|_{\mathcal{N}_{\Phi_\ell}} \leq (C_1 \mu^\theta + C_1 \eta^{-\theta}) \|Ee_{\ell-2}\|_{\mathcal{N}_{\Phi_{\ell-1}}}.$$

Recurring  $\ell - 2$  times, we arrive at the bound

$$\begin{aligned} \|w_\ell\|_{\mathcal{N}_{\Phi_\ell}} &\leq \|Ee_{\ell-1}\|_{\mathcal{N}_{\Phi_\ell}} \leq (C_1 \mu^\theta + C_1 \eta^{-\theta})^{\ell-2} \|Ee_0\|_{\mathcal{N}_{\Phi_1}} \\ &= (C_1 \mu^\theta + C_1 \eta^{-\theta})^{\ell-2} \|Ef\|_{\mathcal{N}_{\Phi_1}} \\ &\leq C_E (C_1 \mu^\theta + C_1 \eta^{-\theta})^{\ell-2} \delta_1^{-\theta} \|f\|_{H^\theta(\Omega)}. \end{aligned}$$

By this bound and by employing the summation formula for the geometric series, we finally estimate

$$\begin{aligned} \sum_{\ell=1}^L \|w_\ell\|_{\mathcal{N}_{\Phi_\ell}}^2 &\leq \sum_{\ell=1}^L C_E^2 c (C_1 \mu^\theta + C_1 \eta^{-\theta})^{2(\ell-2)} \delta_1^{-2\theta} \|f\|_{H^\theta(\Omega)}^2 \\ &= \frac{C_E^2 \delta_1^{-2\theta}}{(C_1 \mu^\theta + C_1 \eta^{-\theta})^2} \|f\|_{H^\theta(\Omega)}^2 \sum_{\ell=0}^{L-1} (C_1 \mu^\theta + C_1 \eta^{-\theta})^{2\ell} \\ &= \frac{C_E^2 \delta_1^{-2\theta}}{(C_1 \mu^\theta + C_1 \eta^{-\theta})^2} \frac{1 - (C_1 \mu^\theta + C_1 \eta^{-\theta})^{2L}}{1 - (C_1 \mu^\theta + C_1 \eta^{-\theta})^2} \|f\|_{H^\theta(\Omega)}^2. \end{aligned}$$

This completes the proof.  $\square$

Combining the previous lemmata with Theorem 2.1, we arrive at the final error estimate.



**Theorem 4.6.** *Under the conditions of Theorems 2.1 and 4.3, there exists a constant  $C > 0$  such that*

$$\|f - \widehat{s}_L\|_{L^2(\Omega)} \leq C \left( (C_1\mu^\theta + C_1\eta^{-\theta})^L + \sqrt{L} \frac{\|\mathcal{K}_{\text{pc}} - \widehat{\mathcal{K}}_{\text{pc}}\|_F}{\|\mathcal{K}_{\text{pc}}\|_F} \right) \|f\|_{H^\theta(\Omega)}.$$

*Proof.* By the triangle inequality, there holds

$$\|f - \widehat{s}_L\|_{L^2(\Omega)} \leq \|f - s_L\|_{L^2(\Omega)} + \|s_L - \widehat{s}_L\|_{L^2(\Omega)}.$$

The first term on the right hand side is bounded using Theorem 2.1. For the second term, we obtain using Lemmata 4.4 and 4.5 as well as Theorem 4.3 that

$$\begin{aligned} \|s_L - \widehat{s}_L\|_{L^2(\Omega)}^2 &\leq CL \sum_{\ell=1}^L \|w_\ell - \widehat{w}_\ell\|_{\mathcal{N}_{\Phi_\ell}}^2 \leq CL \frac{\|\mathcal{K}_{\text{pc}} - \widehat{\mathcal{K}}_{\text{pc}}\|_F^2}{\|\mathcal{K}_{\text{pc}}\|_F^2} \sum_{\ell=1}^L \|w_\ell\|_{\mathcal{N}_{\Phi_\ell}}^2 \\ &\leq CL \frac{\|\mathcal{K}_{\text{pc}} - \widehat{\mathcal{K}}_{\text{pc}}\|_F^2}{\|\mathcal{K}_{\text{pc}}\|_F^2} \|f\|_{H^\theta(\Omega)}^2. \end{aligned}$$

Taking square roots and inserting into the first inequality yields the claim.  $\square$

## 5. SAMPLETS FOR SCATTERED DATA APPROXIMATION

Samplets are discrete signed measures, which exhibit vanishing moments. We briefly recall their underlying concepts as introduced in [9]. To this end, we consider the image of the spaces  $\mathcal{S}_\ell$ ,  $\ell = 1, \dots, L$ , defined in Equation (7), under the Riesz isomorphism  $\mathcal{J}: \mathcal{N}_{\Phi_\ell} \rightarrow \mathcal{N}'_{\Phi_\ell}$  and define

$$(14) \quad \mathcal{S}'_\ell := \text{span}\{\mathcal{J}\Phi_\ell(\cdot - \mathbf{x}) : \mathbf{x} \in X_\ell\} = \text{span}\{\delta_{\mathbf{x}} : \mathbf{x} \in X_\ell\},$$

by the identity  $\mathcal{J}\Phi_\ell(\cdot - \mathbf{x}) = \delta_{\mathbf{x}}$ , where  $\delta_{\mathbf{x}}$  is the point evaluation functional at  $\mathbf{x} \in \Omega$ . We equip the spaces  $\mathcal{S}'_\ell$  with an inner product, different from the canonical one, by the defining property  $\langle \delta_{\mathbf{x}_i}, \delta_{\mathbf{x}_j} \rangle_{\mathcal{S}'_\ell} := \delta_{ij}$  for  $\mathbf{x}_i, \mathbf{x}_j \in X_\ell$ .

For the sake of a more lightweight notation, we drop the subscript  $\ell$  of the spaces  $\mathcal{S}'_\ell$  for the remainder of this paragraph and remark that each space  $\mathcal{S}'_\ell$  will in general have a different multiresolution analysis, where the maximum level  $J$  depends on  $\ell$ . Given a multiresolution analysis  $\mathcal{V}'_0 \subset \mathcal{V}'_1 \subset \dots \subset \mathcal{V}'_J = \mathcal{S}'$ , we keep track of the increment of information between two consecutive levels  $j$  and  $j+1$ . Since there holds  $\mathcal{V}'_j \subset \mathcal{V}'_{j+1}$ , we may orthogonally decompose  $\mathcal{V}'_{j+1} = \mathcal{V}'_j \oplus \mathcal{W}'_j$  for a certain *detail space*  $\mathcal{W}'_j \perp \mathcal{V}'_j$ . In analogy to wavelet nomenclature, we call the elements of a basis of  $\mathcal{V}'_0$  *scaling distributions* and the elements of a basis of one of the spaces  $\mathcal{W}'_j$  *samplets*. This name is motivated by the idea that the basis distributions in  $\mathcal{W}'_j$  are supported at a small subsample or samplet of the data sites in  $X$ . The collection of the bases of  $\mathcal{W}'_j$  for  $j = 0, \dots, J-1$  together with a basis of  $\mathcal{V}'_0$  is called a *samplet basis* for  $\mathcal{S}'$ . A samplet basis can be constructed such that it exhibits *vanishing moments* of order  $q+1$ , i.e.,

$$(15) \quad \sigma_{j,k}(p) = 0 \quad \text{for all } p \in \mathcal{P}_q,$$

where  $\sigma_{j,k} \in \mathcal{W}'_j$  is a samplet and  $\mathcal{P}_q := \text{span}\{\mathbf{x}^\alpha : \|\alpha\|_1 \leq q\}$  denotes the space of polynomials of total degree at most  $q$ .

The samplet construction for  $\mathcal{S}'$  is based on a *cluster tree* for the set of data sites  $X$ , i.e., a tree  $\mathcal{C}$  with root  $X$  such that each node  $\tau \in \mathcal{C}$  is the disjoint union of its children. Such a cluster tree  $\mathcal{C}$  directly induces a support based hierarchical clustering of the subspace  $\mathcal{S}'$ , spanned by the Dirac- $\delta$ -distributions supported at the data sites in  $X$ . With a slight abuse of notation, we will refer to this cluster tree also by  $\mathcal{C}$  and to its nodes by  $\tau$ . Given a cluster tree  $\mathcal{C}$ , a samplet basis for  $\mathcal{S}'$ , where  $\dim \mathcal{S}' = N$ , can be constructed with cost  $\mathcal{O}(N)$ . Assuming furthermore, that  $\mathcal{C}$  is a balanced binary tree with maximum level  $J = \lceil \log_2(N) \rceil$ , the samplet basis exhibits the following properties, see [9] but also [8, 25].

**Theorem 5.1.** *The samplet basis  $\bigcup_{j=0}^J \{\sigma_{j,k}\}_k$  forms an orthonormal basis in  $\mathcal{S}'$ , satisfying the following properties:*

- (1) There holds  $c^{-1}2^j \leq \dim \mathcal{W}'_j \leq c2^j$  for a constant  $1 < c \leq 2$ .
- (2) The samplelets have vanishing moments of order  $q+1$ , i.e.,  $(p, \sigma_{j,k})_\Omega = 0$  for all  $p \in \mathcal{P}_q(\Omega)$ , where  $\mathcal{P}_q(\Omega)$  is the space of polynomials up to degree  $q$ .
- (3) The coefficient vector  $\boldsymbol{\omega}_{j,k} = [\omega_{j,k,i}]_i$  of the samplelet  $\sigma_{j,k}$  satisfies the bound  $\|\boldsymbol{\omega}_{j,k}\|_1 \leq c2^{(J-j)/2}$  for a constant  $0 < c < 2$ .
- (4) Given  $f \in C^{q+1}(O)$ , for some open set  $O \supset \text{supp } \sigma_{j,k}$ , there holds

$$|\sigma_{j,k}(f)| \leq \left(\frac{d}{2}\right)^{q+1} \frac{(\text{diam supp } \sigma_{j,k})^{q+1}}{(q+1)!} \|f\|_{C^{q+1}(O)} \|\boldsymbol{\omega}_{j,k}\|_1.$$

- (5) For quasi-uniform sets  $X$ , there holds  $\text{diam supp } \sigma_{j,k} \leq c2^{-j/d}$  for some constant  $c > 0$ .

A direct consequence of the orthonormality of the samplelet basis is that the samplelet transform  $[\sigma_{j,k}]_{j,k} = \mathbf{T}[\delta_{\mathbf{x}_i}]_{i=1}^N$  satisfies  $\mathbf{T}^\top \mathbf{T} = \mathbf{T} \mathbf{T}^\top = \mathbf{I} \in \mathbb{R}^{N \times N}$ . If the samplelet transform  $\mathbf{T}$  is computed recursively adhering the hierarchy induced by the cluster tree  $\mathcal{C}$ , its cost is of order  $\mathcal{O}(N)$ .

Employing the Riesz isometry, the samplelet basis induces a basis for  $\mathcal{S} \subset \mathcal{N}_\Phi$ . To this end, consider a samplelet  $\sigma_{j,k} = \sum_{i=1}^N \omega_{j,k,i} \delta_{\mathbf{x}_i}$ . The samplelet can be identified with the function  $\psi_{j,k} := \sum_{i=1}^N \omega_{j,k,i} \Phi(\mathbf{x}_i - \cdot) \in \mathcal{S}$  by means of the Riesz isometry. The vanishing moment property (15) then translates to  $\langle \psi_{j,k}, f \rangle_{\mathcal{N}_\Phi} = 0$  for any  $f \in \mathcal{N}_\Phi$  which satisfies  $f|_{\text{supp}(\sigma_{j,k})} \in \mathcal{P}_q$ .

Furthermore, there holds

$$(16) \quad [\langle \psi_{j,k}, \psi_{j',k'} \rangle_{\mathcal{N}_\Phi}]_{j,j',k,k'} = \mathbf{T} \mathbf{K} \mathbf{T}^\top =: \mathbf{K}^\Sigma.$$

This means that the Gramian of the embedded samplelet basis in  $\mathcal{S}$  is just the samplelet transformed generalized Vandermonde matrix. For *asymptotically smooth* kernels  $K$ , i.e., there exist  $C, r > 0$  such that for all  $(\mathbf{x}, \mathbf{y}) \in (\Omega \times \Omega) \setminus \Delta$

$$(17) \quad \left| \frac{\partial^{|\boldsymbol{\alpha}|+|\boldsymbol{\beta}|}}{\partial \mathbf{x}^\boldsymbol{\alpha} \partial \mathbf{y}^\boldsymbol{\beta}} K(\mathbf{x}, \mathbf{y}) \right| \leq C \frac{(|\boldsymbol{\alpha}|+|\boldsymbol{\beta}|)!}{r^{|\boldsymbol{\alpha}|+|\boldsymbol{\beta}|} \|\mathbf{x} - \mathbf{y}\|_2^{|\boldsymbol{\alpha}|+|\boldsymbol{\beta}|}}$$

uniformly in  $\boldsymbol{\alpha}, \boldsymbol{\beta} \in \mathbb{N}^d$  apart from the diagonal  $\Delta := \{(\mathbf{x}, \mathbf{y}) \in \Omega \times \Omega : \mathbf{x} = \mathbf{y}\}$ , the matrix  $\mathbf{K}^\Sigma$  becomes quasi-sparse and can efficiently be computed. More precisely, a compression based on cluster distances is applied to compute a sparsified version of the matrix  $\mathbf{K}^\Sigma$ . In detail, there holds the following result, see [9].

**Theorem 5.2.** *Let  $X$  be quasi-uniform with  $\#X = N$  and set all coefficients of the generalized Vandermonde matrix  $\mathbf{K}^\Sigma$  from (16) to zero which satisfy the admissibility condition*

$$(18) \quad \text{dist}(\tau, \tau') \geq \rho \max\{\text{diam}(\tau), \text{diam}(\tau')\}, \quad \rho > 0,$$

where  $\tau$  is the cluster supporting  $\sigma_{j,k}$  and  $\tau'$  is the cluster supporting  $\sigma_{j',k'}$ , respectively. Then, there exists a constant  $C > 0$ , such that the resulting compressed matrix  $\mathbf{K}^{\Sigma, \rho}$  satisfies

$$(19) \quad \frac{\|\mathbf{K}^\Sigma - \mathbf{K}^{\Sigma, \rho}\|_F}{\|\mathbf{K}^\Sigma\|_F} \leq C m_q \left(\frac{r\rho}{d}\right)^{-2(q+1)},$$

where  $m_q = \binom{q+d}{d}$  is the dimension of  $\mathcal{P}_q$ . The compressed matrix has  $\mathcal{O}(m_q^2 N \log N)$  nonzero coefficients.

We remark that, given a radial function satisfying (17), the corresponding scaled kernel (6) satisfies the asymptotical smoothness estimate, cp. [10],

$$\left| \frac{\partial^{|\boldsymbol{\alpha}|+|\boldsymbol{\beta}|}}{\partial \mathbf{x}^\boldsymbol{\alpha} \partial \mathbf{y}^\boldsymbol{\beta}} K_\ell(\mathbf{x}, \mathbf{y}) \right| \leq C \delta_\ell^{-d} \frac{(|\boldsymbol{\alpha}|+|\boldsymbol{\beta}|)!}{(r\delta_\ell)^{|\boldsymbol{\alpha}|+|\boldsymbol{\beta}|} \|\mathbf{x} - \mathbf{y}\|_2^{|\boldsymbol{\alpha}|+|\boldsymbol{\beta}|}} = C \delta_\ell^{-d} \frac{(|\boldsymbol{\alpha}|+|\boldsymbol{\beta}|)!}{r^{|\boldsymbol{\alpha}|+|\boldsymbol{\beta}|} \|\mathbf{x} - \mathbf{y}\|_2^{|\boldsymbol{\alpha}|+|\boldsymbol{\beta}|}},$$

which means that the dependency of the derivatives on  $\delta_\ell$  just cancels out. Moreover, we remark that, since we only require derivatives of the kernel up to order  $2q+1$  to be bounded, the asymptotical smoothness requirement could in principle also be weakened to kernels of finite smoothness, see, e.g., [11] for details.

## 6. MULTISCALE ALGORITHM IN SAMPLET COORDINATES

In this section, we transform the interpolation problem from the original basis, referred to as the *kernel basis*, to the samplet basis, as introduced in Section 5. In what follows, we denote the samplet transform for  $\mathcal{S}'_\ell$  by  $\mathbf{T}_\ell \in \mathbb{R}^{N_\ell \times N'_\ell}$  and recall that  $\mathbf{T}_\ell^\top \mathbf{T}_\ell = \mathbf{T}_\ell \mathbf{T}_\ell^\top = \mathbf{I} \in \mathbb{R}^{N_\ell \times N_\ell}$ . Defining the block transform  $\mathcal{T} := \text{diag}(\mathbf{T}_1, \dots, \mathbf{T}_L)$  there holds  $\mathcal{T}^\top \mathcal{T} = \mathcal{T} \mathcal{T}^\top = \mathbf{I}$ . Hence, the linear system (10) is equivalent to

$$\mathcal{T}^\top \mathcal{T} \begin{bmatrix} \mathbf{K}_{1,1} & & & \\ \mathbf{K}_{2,1} & \mathbf{K}_{2,2} & & \\ \vdots & \vdots & \ddots & \\ \mathbf{K}_{L,1} & \mathbf{K}_{L,2} & \cdots & \mathbf{K}_{L,L} \end{bmatrix} \mathcal{T}^\top \mathcal{T} \begin{bmatrix} \mathbf{c}_1 \\ \mathbf{c}_2 \\ \vdots \\ \mathbf{c}_L \end{bmatrix} = \mathcal{T}^\top \mathcal{T} \begin{bmatrix} \mathbf{f}_1 \\ \mathbf{f}_2 \\ \vdots \\ \mathbf{f}_L \end{bmatrix}.$$

Letting  $\mathbf{K}_{\ell,\ell'}^\Sigma := \mathbf{T}_\ell \mathbf{K}_{\ell,\ell'} \mathbf{T}_{\ell'}^\top \in \mathbb{R}^{N_\ell \times N'_{\ell'}}$ ,  $\mathbf{c}_\ell^\Sigma := \mathbf{T}_\ell \mathbf{c}_\ell \in \mathbb{R}^{N_\ell}$ ,  $\mathbf{f}_\ell^\Sigma := \mathbf{T}_\ell \mathbf{f}_\ell \in \mathbb{R}^{N_\ell}$ , we can rewrite the previous system according to

$$(20) \quad \begin{bmatrix} \mathbf{K}_{1,1}^\Sigma & & & \\ \mathbf{K}_{2,1}^\Sigma & \mathbf{K}_{2,2}^\Sigma & & \\ \vdots & \vdots & \ddots & \\ \mathbf{K}_{L,1}^\Sigma & \mathbf{K}_{L,2}^\Sigma & \cdots & \mathbf{K}_{L,L}^\Sigma \end{bmatrix} \begin{bmatrix} \mathbf{c}_1^\Sigma \\ \mathbf{c}_2^\Sigma \\ \vdots \\ \mathbf{c}_L^\Sigma \end{bmatrix} = \begin{bmatrix} \mathbf{f}_1^\Sigma \\ \mathbf{f}_2^\Sigma \\ \vdots \\ \mathbf{f}_L^\Sigma \end{bmatrix}.$$

Since  $\mathcal{T}$  is an isometry, the condition number of this system is identical to that of (10). In particular, the diagonal blocks remain well-conditioned in accordance with Corollary 3.2. Applying the matrix compression from Theorem 5.2 to each of the blocks  $\mathbf{K}_{\ell,\ell'}^\Sigma$ , we arrive at the compressed, samplet transformed system

$$(21) \quad \begin{bmatrix} \mathbf{K}_{1,1}^{\Sigma,\rho} & & & \\ \mathbf{K}_{2,1}^{\Sigma,\rho} & \mathbf{K}_{2,2}^{\Sigma,\rho} & & \\ \vdots & \vdots & \ddots & \\ \mathbf{K}_{L,1}^{\Sigma,\rho} & \mathbf{K}_{L,2}^{\Sigma,\rho} & \cdots & \mathbf{K}_{L,L}^{\Sigma,\rho} \end{bmatrix} \begin{bmatrix} \mathbf{c}_1^\Sigma \\ \mathbf{c}_2^\Sigma \\ \vdots \\ \mathbf{c}_L^\Sigma \end{bmatrix} = \begin{bmatrix} \mathbf{f}_1^\Sigma \\ \mathbf{f}_2^\Sigma \\ \vdots \\ \mathbf{f}_L^\Sigma \end{bmatrix}.$$

A detailed algorithm for solving (21) using block forward substitution and evaluating the resulting approximation at a set of points can be found in Algorithm (1). We remark that replacing the kernel matrix for the evaluation points by its samplet compressed version leads to a further consistency error, which can, however, be bounded with similar ideas as in Lemma 4.1.

**Algorithm 1** Multiscale interpolation in samplet coordinates

**Input:** Sets of points  $\{X_1, \dots, X_L\}$ , function  $f$ , parameters  $\rho, q$ .  
**Output:** Coefficient vectors  $\widehat{\mathbf{c}}_1, \dots, \widehat{\mathbf{c}}_L$  corresponding to  $\widehat{w}_1, \dots, \widehat{w}_L$ .

```

1: for  $\ell = 1, 2, \dots, L$  do
2:   Compute  $\mathbf{f}_\ell^\Sigma \leftarrow \mathbf{T}_\ell \mathbf{f}_\ell := f|_{X_\ell}$ .
3:   for  $\ell' = 1, 2, \dots, \ell$  do
4:     Compute  $\mathbf{K}_{\ell,\ell'}^{\Sigma,\rho}$  using  $q + 1$  vanishing moments.
5:   end for
6:   Compute  $\widehat{\mathbf{e}}_\ell^\Sigma \leftarrow \mathbf{f}_\ell^\Sigma - \sum_{\ell'=1}^{\ell-1} \mathbf{K}_{\ell,\ell'}^{\Sigma,\rho} \widehat{\mathbf{c}}_{\ell'}^\Sigma$ .
7:   Solve the local interpolation problem  $\mathbf{K}_{\ell,\ell}^{\Sigma,\rho} \widehat{\mathbf{c}}_\ell^\Sigma = \widehat{\mathbf{e}}_\ell^\Sigma$ .
8:   Compute  $\widehat{\mathbf{c}}_\ell \leftarrow \mathbf{T}_\ell^\top \widehat{\mathbf{c}}_\ell^\Sigma$ .
9: end for

```

The overall compression error of (21), can be estimated by summing up the block-wise errors in accordance with Theorem 5.2. The following result is immediate.

**Theorem 6.1.** *Let  $X_1, \dots, X_L$  be quasi-uniform. Then, the compression error in the linear system (21) can be bounded according to*

$$\frac{\|\mathcal{K}^\Sigma - \mathcal{K}^{\Sigma, \rho}\|_F}{\|\mathcal{K}^\Sigma\|_F} \leq C m_q (r\rho/d)^{-2(q+1)},$$

where we denote the block matrix from (20) by  $\mathcal{K}^\Sigma$  and the one from (21) by  $\mathcal{K}^{\Sigma, \rho}$ , respectively.

Observing that  $\mathcal{T}\mathcal{D}^{1/2} = \mathcal{D}^{1/2}\mathcal{T}$ , combining the previous theorem with Theorem 4.6 immediately results in an error estimate for the approximation  $\widehat{s}_L$  to  $s_L$  obtained by solving the samplelet compressed system.

**Theorem 6.2.** *Let the conditions of Theorem 4.6 be satisfied. Then, the numerical approximation  $\widehat{s}_L$  resulting from solving (21) satisfies the error estimate*

$$\|f - \widehat{s}_L\|_{L^2(\Omega)} \leq C \left( (C_1 \mu^\theta + C_1 \eta^{-\theta})^L + \sqrt{L} m_q (r\rho/d)^{-2(q+1)} \right) \|f\|_{H^\theta(\Omega)}.$$

Finally, we have the subsequent result on the cost of our multiscale algorithm, which is in line with a similar result for multiscale interpolation using hierarchical matrices, see [14].

**Theorem 6.3.** *Let  $X_1, \dots, X_L$  be quasi-uniform and assume that the corresponding cardinalities  $\{N_\ell\}_\ell$  form a geometric sequence, i.e.,  $N_1 > 0$  and  $N_\ell = c_{\text{geo}}^\ell N_1$  for some constant  $c_{\text{geo}} > 1$ . Then, the overall computational cost for assembling the linear system (21) and the number of non-vanishing matrix entries are both bounded by  $\mathcal{O}(N_L \log^2 N_L)$ , with the hidden constant depending on the dimension  $m_q$  of  $\mathcal{P}_q$ .*

*Proof.* Fix a row index  $\ell$ . It has been shown within [1, Proof of Theorem 3.16] that the cost for the computation of  $\mathbf{K}_{\ell, \ell'}^{\Sigma, \rho}$  amounts to  $\mathcal{O}(N_\ell \log N_{\ell'})$ , which is also the number of non-vanishing entries of that row. Moreover, there are  $\ell$  blocks per row. Hence, the cost for the computation of the  $\ell$ -th row of (21) is given by

$$\sum_{\ell'=1}^{\ell} \mathcal{O}(N_\ell \log N_{\ell'}) = \mathcal{O}\left(N_\ell \sum_{\ell'=1}^{\ell} \log N_{\ell'}\right) = \mathcal{O}(N_\ell \log^2 N_\ell),$$

since  $\ell = \mathcal{O}(\log N_\ell)$  due to the geometric sequence property. Next, summing up the cost of the individual rows yields the overall cost

$$\sum_{\ell=1}^L \mathcal{O}(N_\ell \log^2 N_\ell) = \mathcal{O}\left(\sum_{\ell=1}^L N_\ell \log^2 N_\ell\right) = \mathcal{O}\left(\log^2 N_L \sum_{\ell=1}^L N_\ell\right) = \mathcal{O}(N_L \log^2 N_L),$$

again due to the geometric sequence property, i.e.,  $\sum_{\ell=1}^L N_\ell = \mathcal{O}(N_L)$ . This completes the proof.  $\square$

To give an idea of the sparsity pattern of the samplelet compressed system (21), Figure 1 visualizes the matrix pattern  $\mathbf{K}_{\ell, \ell'}^\Sigma$  using three levels of points  $X_1, X_2, X_3$  arranged on a regular grid for the unit square, with cardinalities of 16 641, 66 049, and 263 169, respectively. Furthermore, we remark that, for a geometric sequence  $\{N_\ell\}_\ell$ , the cost for applying  $\mathcal{T}$  and  $\mathcal{T}^\top$ , respectively, remains linear in  $N_L$ .

## 7. NUMERICAL RESULTS

We present numerical examples of the proposed multiscale interpolation in samplelets coordinates in both two and three dimensional settings. The parameters for the samplelet compression are  $\rho$  and  $q$ . The first one is associated with the admissibility condition (18), which determines the matrix blocks that are initially truncated. A larger  $\rho$  results in a larger distance between clusters before they are admissible for compression. In our analysis, we adopt  $\rho = d$ , so that the bound in Equation (19) is exponentially governed by the number of vanishing moments, denoted as  $q + 1$ , see (15). The higher  $q + 1$ , the more polynomial exactness is gained.

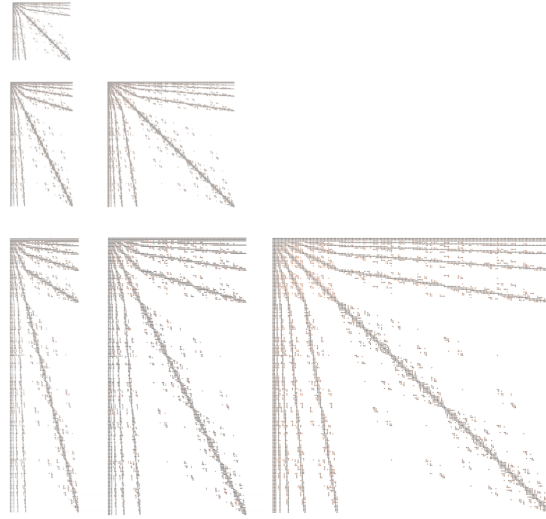


FIGURE 1. Example of the sparsity patterns of the matrices  $\mathbf{K}_{\ell, \ell'}^{\Sigma, \rho}$  for  $\ell, \ell' \in \{1, 2, 3\}$  of the compressed linear system from (21).

In the experiments, we vary also the parameter  $\gamma$ , defined as  $\gamma = \eta\mu$ , where  $\delta$  is the kernel rescaling factor, given by  $\delta_i = \eta h_{X_i}$  and previously defined in (3), while  $\eta$  represents the scaling factor for the fill distance between consecutive levels, i.e.,  $h_{X_{\ell+1}} \approx \mu h_{X_\ell}$ .

To measure the approximation quality, we consider the relative interpolation errors

$$\text{error}_{p,m} = \frac{\|f - \hat{s}_m|_{X_{\text{eval}}}\|_{\ell^p}}{\|f|_{X_{\text{eval}}}\|_{\ell^p}}$$

for  $p = 2$  and  $p = \infty$  at each of the levels  $m = 1, \dots, L$  for a given set of evaluation points  $X_{\text{eval}}$ . Furthermore, we compute the order of convergence, given by

$$\text{order}_{p,m} = \frac{\log\left(\frac{\text{error}_{p,m+1}}{\text{error}_{p,m}}\right)}{\log\left(\frac{h_{m+1}}{h_m}\right)}.$$

We investigate three different scenarios in our numerical tests. The first two are adapted from [29]: a smooth function on the unit square and a non-smooth function on the L-shaped domain. Finally, we extend to a three dimensional setting issuing from the Lucy surface model of the **Stanford 3D Scanning Repository**<sup>1</sup>.

All computations have been performed at the Centro Svizzero di Calcolo Scientifico (CSCS) on a single node of the Alps cluster<sup>2</sup> with two AMD EPYC 7742 @2.25GHz CPUs with 470GB of main memory. For the computations, we have used up to 16 cores. The implementation of the samplelet compression is available as software package **FMCA**<sup>3</sup>.

**7.1. Franke's function in two spatial dimensions.** We interpolate Franke's function, as introduced in [5], defined by

$$(22) \quad \begin{aligned} f(x, y) = & \frac{3}{4} \exp\left(-\frac{(9x-2)^2}{4} - \frac{(9y-2)^2}{4}\right) + \frac{3}{4} \exp\left(-\frac{(9x+1)^2}{49} - \frac{(9y+1)^2}{10}\right) \\ & + \frac{1}{2} \exp\left(-\frac{(9x-7)^2}{4} - \frac{(9y-3)^2}{4}\right) - \frac{1}{5} \exp(-(9x-4)^2 - (9y-7)^2) \end{aligned}$$

<sup>1</sup><https://graphics.stanford.edu/data/3Dscanrep/>

<sup>2</sup><https://www.cscs.ch/computers/alps>

<sup>3</sup><https://github.com/muchip/fmca>

on the unit square  $\Omega = [0, 1]^2$ . To this end, we generate 10 sets of nested points within this domain, distributing them on a regular grid with size  $h_\ell = 2^{-\ell}$ . The number of points per level and the corresponding fill-distances are provided in Table 1.

$\ell$	$N_\ell$	$h$
1	9	0.5
2	25	0.25
3	81	0.125
4	289	0.0625
5	1 089	0.03125
6	4 225	0.015625
7	16 641	0.0078125
8	66 049	0.00390625
9	263 169	0.00195312
10	1 050 625	0.000976562

TABLE 1. Number of points per level and the corresponding fill-distances on  $\Omega = [0, 1]^2$  for the interpolation of Franke’s function.

The solution is approximated with the  $C^1$ -smooth Matérn-3/2 RBF and the  $C^2$ -smooth Matérn-5/2 RBF for different values of  $\gamma$  and using  $\rho = 2$ ,  $q = 4$ . Furthermore, we perform an a-posteriori thresholding of small matrix entries with a relative threshold of  $10^{-8}$  with respect to the Frobenius norm, cp. Theorem 6.1. The error is evaluated at a fine grid with mesh-size  $h = 2^{-11}$ . The accuracy of the conjugate gradient method is set to  $10^{-6}$ . Increasing the accuracy does not result in smaller errors but increases the number of iterations. Interpolation error, order, and compression rate (measured as the percentage of nonzero entries, %nz), as well as (non-preconditioned) conjugate gradient iterations (CG), are presented in Tables 2–5.

$\ell$	Matérn-3/2 RBF							
	$\gamma = 0.25$				$\gamma = 0.5$			
	error <sub>2</sub>	order <sub>2</sub>	%nz	CG	error <sub>2</sub>	order <sub>2</sub>	%nz	CG
1	$5.67 \cdot 10^{-1}$	–	55	5	$4.84 \cdot 10^{-1}$	–	55	6
2	$1.38 \cdot 10^{-1}$	2.04	40	8	$5.29 \cdot 10^{-2}$	2.19	40	13
3	$3.16 \cdot 10^{-2}$	2.12	43	9	$9.20 \cdot 10^{-3}$	2.53	43	25
4	$6.76 \cdot 10^{-3}$	2.23	48	10	$1.15 \cdot 10^{-3}$	3.00	48	34
5	$1.48 \cdot 10^{-3}$	2.19	22	10	$2.51 \cdot 10^{-4}$	2.53	28	39
6	$3.45 \cdot 10^{-4}$	2.10	7.8	10	$6.08 \cdot 10^{-5}$	2.05	10	39
7	$8.30 \cdot 10^{-5}$	2.06	2.3	10	$1.30 \cdot 10^{-5}$	2.22	3.2	39
8	$1.46 \cdot 10^{-5}$	2.51	0.64	10	$1.14 \cdot 10^{-6}$	3.51	0.89	39
9	$3.13 \cdot 10^{-6}$	2.22	0.17	10	$9.98 \cdot 10^{-8}$	3.52	0.23	39
10	$7.85 \cdot 10^{-7}$	2.00	0.04	10	$3.47 \cdot 10^{-8}$	1.52	0.06	39

TABLE 2. Results for the interpolation of Franke’s function using the  $C^1$ -smooth Matérn-3/2 RBF and  $\rho = 2$ ,  $q = 4$  as samplet compression parameters.

The tables clearly demonstrate the expected exponential decay of the approximation error with increasing level for both error measures and both RBFs under consideration. Furthermore, we see the effect of a larger value of  $\gamma$ , which corresponds to a larger lengthscale parameter of the RBF, resulting in a larger condition number. For increasing  $\gamma$ , we require successively more iterations for the conjugate gradient method to achieve the prescribed accuracy, with up to 430 iterations for  $\gamma = 1$  and the Matérn-5/2 RBF.

Matérn-3/2 RBF								
$\gamma = 0.75$					$\gamma = 1$			
$\ell$	error <sub>2</sub>	order <sub>2</sub>	%nz	CG	error <sub>2</sub>	order <sub>2</sub>	%nz	CG
1	$4.84 \cdot 10^{-1}$	—	55	6	$4.88 \cdot 10^{-1}$	—	55	6
2	$4.67 \cdot 10^{-2}$	3.37	40	17	$4.51 \cdot 10^{-2}$	3.43	40	20
3	$7.97 \cdot 10^{-3}$	2.55	43	40	$7.72 \cdot 10^{-3}$	2.55	43	48
4	$5.70 \cdot 10^{-4}$	3.81	48	63	$3.60 \cdot 10^{-4}$	4.43	48	96
5	$1.09 \cdot 10^{-4}$	2.38	35	90	$5.75 \cdot 10^{-5}$	3.31	37	155
6	$2.38 \cdot 10^{-5}$	2.19	14	96	$1.16 \cdot 10^{-5}$	2.31	15	186
7	$4.57 \cdot 10^{-6}$	2.38	4.4	98	$2.06 \cdot 10^{-6}$	2.49	5.0	195
8	$4.74 \cdot 10^{-7}$	3.26	1.2	99	$2.16 \cdot 10^{-7}$	3.25	1.4	196
9	$3.80 \cdot 10^{-8}$	3.64	0.32	98	$3.05 \cdot 10^{-8}$	2.83	0.38	197
10	$1.33 \cdot 10^{-8}$	1.51	0.08	98	$1.41 \cdot 10^{-8}$	1.11	0.09	200

TABLE 3. Results for the interpolation of Franke’s function using the  $C^1$ -smooth Matérn-3/2 RBF and  $\rho = 2$ ,  $q = 4$  as samplelet compression parameters.

Matérn-5/2 RBF								
$\gamma = 0.25$					$\gamma = 0.5$			
$\ell$	error <sub>2</sub>	order <sub>2</sub>	%nz	CG	error <sub>2</sub>	order <sub>2</sub>	%nz	CG
1	$5.45 \cdot 10^{-1}$	—	55	5	$4.72 \cdot 10^{-1}$	—	55	6
2	$1.12 \cdot 10^{-1}$	2.28	40	8	$4.51 \cdot 10^{-2}$	1.39	40	16
3	$2.27 \cdot 10^{-2}$	2.14	43	9	$7.77 \cdot 10^{-3}$	2.54	43	32
4	$4.54 \cdot 10^{-3}$	2.32	48	10	$6.92 \cdot 10^{-4}$	3.48	48	42
5	$1.00 \cdot 10^{-3}$	2.18	22	10	$1.49 \cdot 10^{-4}$	2.21	25	48
6	$2.49 \cdot 10^{-4}$	2.01	7.8	10	$3.42 \cdot 10^{-5}$	2.12	8.8	48
7	$6.13 \cdot 10^{-5}$	2.02	2.3	10	$6.88 \cdot 10^{-6}$	2.31	2.7	48
8	$6.06 \cdot 10^{-6}$	3.34	0.64	9	$8.31 \cdot 10^{-7}$	3.05	0.74	48
9	$1.15 \cdot 10^{-6}$	2.40	0.17	9	$5.68 \cdot 10^{-8}$	3.87	0.19	48
10	$3.07 \cdot 10^{-7}$	1.91	0.04	9	$6.86 \cdot 10^{-9}$	3.05	0.05	48

TABLE 4. Results for the interpolation of Franke’s function using the  $C^2$ -smooth Matérn-5/2 RBF and  $\rho = 2$ ,  $q = 4$  as samplelet compression parameters.

To validate the theoretical bound on the computational cost of assembling the linear system stated in Theorem 2.1, Figure 2 shows the single threaded computation times obtained with  $\gamma = 1$  and the Matérn-3/2 RBF. The dashed lines correspond to the rates  $N \log^\alpha N$  for  $\alpha = 1, 2, 3$ . The results clearly confirm that the overall time scales as  $N \log^2 N$ , in agreement with the theoretical analysis. Finally, Figure 3 shows a visualization of the solution (left) and the residuals (right) at levels  $\ell = 1, 4, 7, 10$  for  $\gamma = 0.5$  using the Matérn-3/2 RBF.

**7.2. Non-smooth function.** We consider the L-shaped domain  $\Omega = [-\frac{1}{2}, \frac{1}{2}]^2 \setminus (0, \frac{1}{2}]^2$  where we introduce polar coordinates  $x = r \cos \phi$ ,  $y = r \sin \phi$ , with  $r \geq 0$  and  $\phi \in [\pi/2, 2\pi]$ . In this test, we aim at interpolating the function  $u(r, \phi) = -r^{\frac{2}{3}} \sin\left(\frac{2\phi - \pi}{3}\right)$ , which solves the Laplace equation  $\Delta u = 0$ . We select  $h_\ell = 2^{-\ell}$  as before. Given the reduced smoothness of the function, we choose the  $C^0$ -smooth Matérn-1/2 RBF for its approximation. The error is evaluated on a fine grid with mesh size  $h = 2^{-9}$ . The parameters for the samplelet matrix compression and the accuracy of the conjugate gradient method are the same as in the previous example. Table 6 provides the number of points per level along with the corresponding fill distances. The results for  $\gamma = 0.5$  and  $\gamma = 1$  are summarized in Table 7.

Matérn-5/2 RBF								
$\gamma = 0.75$					$\gamma = 1$			
$\ell$	error <sub>2</sub>	order <sub>2</sub>	%nz	CG	error <sub>2</sub>	order <sub>2</sub>	%nz	CG
1	$4.79 \cdot 10^{-1}$	—	55	6	$9.16 \cdot 10^{-1}$	—	55	7
2	$4.41 \cdot 10^{-2}$	3.44	40	20	$4.69 \cdot 10^{-2}$	4.29	40	25
3	$7.13 \cdot 10^{-3}$	2.63	43	58	$7.47 \cdot 10^{-3}$	2.65	43	83
4	$3.29 \cdot 10^{-4}$	4.43	48	96	$1.63 \cdot 10^{-4}$	2.19	48	171
5	$6.14 \cdot 10^{-5}$	2.42	35	139	$3.96 \cdot 10^{-5}$	2.04	37	301
6	$1.22 \cdot 10^{-5}$	2.33	13	155	$1.34 \cdot 10^{-5}$	1.56	15	369
7	$2.11 \cdot 10^{-6}$	2.53	4.2	157	$2.06 \cdot 10^{-6}$	2.70	4.8	403
8	$2.57 \cdot 10^{-7}$	3.03	1.2	158	$2.39 \cdot 10^{-7}$	3.10	1.4	407
9	$4.06 \cdot 10^{-8}$	2.66	0.31	159	$7.56 \cdot 10^{-8}$	1.66	0.36	436
10	$3.04 \cdot 10^{-8}$	0.42	0.08	162	$7.01 \cdot 10^{-8}$	0.11	0.09	430

TABLE 5. Results for the interpolation of Franke’s function using the  $C^2$ -smooth Matérn-5/2 RBF and  $\rho = 2$ ,  $q = 4$  as samplet compression parameters.

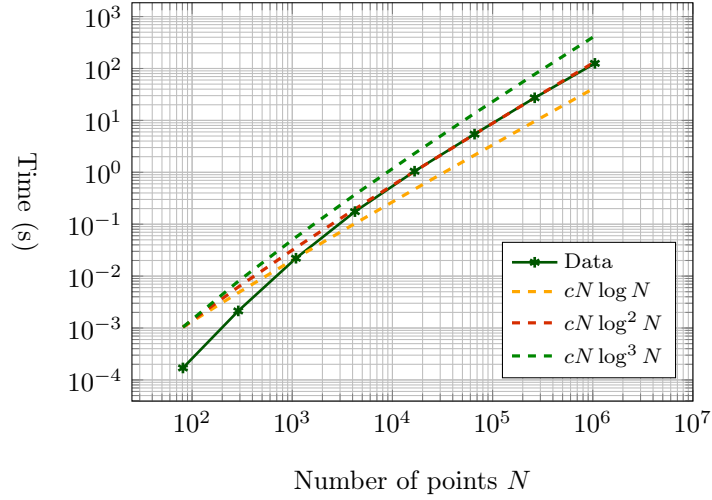


FIGURE 2. Comparison of the overall assembly time (blue) with theoretical growth rates  $N \log^\alpha N$  for  $\alpha = 1, 2, 3$ .

$\ell$	$N_\ell$	$h$
1	21	0.25
2	65	0.125
3	225	0.0625
4	833	0.03125
5	3 201	0.015625
6	12 545	0.0078125
7	49 665	0.00390625
8	197 633	0.00195312

TABLE 6. Number of points per level and the corresponding fill-distances on the L-shaped domain for the interpolation of the solution to the Laplace equation.

The compression rates are similar to the previous example, also in case of the less smooth Matérn-1/2 RBF. The approximation error and the corresponding order are reduced, however.



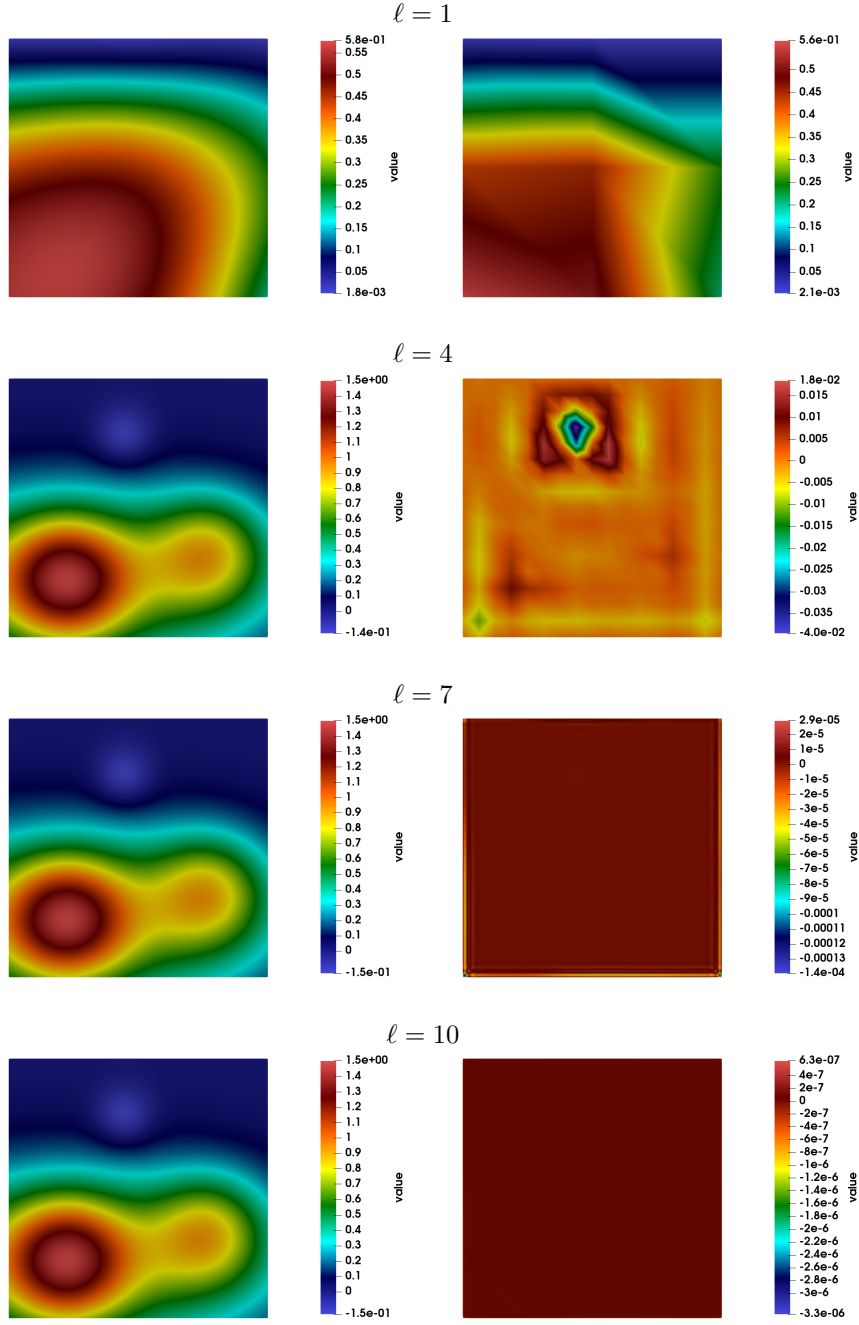


FIGURE 3. Solution (left) and corresponding residuals (right) for the interpolation of Franke's function for levels  $\ell = 1, 4, 7, 10$ .

The number of conjugate gradient iterations stays rather low with a maximum of 28 iterations for  $\gamma = 0.5$  and of 79 iterations for  $\gamma = 1$ . This can be explained by the slower decay of the Matérn-1/2 kernel's eigenvalues, resulting in less ill-conditioned generalized Vandermonde matrices.

Figure 4 illustrates the solution (left) and the corresponding residuals (right) at levels  $\ell = 2, 4, 6, 8$  with  $\gamma = 0.5$ .

**7.3. Function on a point cloud in three spatial dimensions.** As final example, we consider a function defined on a uniform resampling of the Lucy surface model of the **Stanford 3D Scanning Repository**. To construct the local approximation spaces, we selected random subsamples of the

$\gamma = 0.5$						
$\ell$	error <sub>2</sub>	error <sub>∞</sub>	order <sub>2</sub>	order <sub>∞</sub>	%nz	CG
1	$4.37 \cdot 10^{-2}$	$5.98 \cdot 10^{-2}$	—	—	52	8
2	$1.38 \cdot 10^{-2}$	$3.17 \cdot 10^{-2}$	1.66	0.92	49	15
3	$5.33 \cdot 10^{-3}$	$2.04 \cdot 10^{-2}$	1.37	0.64	38	22
4	$1.83 \cdot 10^{-3}$	$1.29 \cdot 10^{-2}$	1.54	0.66	18	25
5	$5.88 \cdot 10^{-4}$	$8.15 \cdot 10^{-3}$	1.64	0.66	6.2	27
6	$1.85 \cdot 10^{-4}$	$5.06 \cdot 10^{-3}$	1.67	0.69	1.8	28
7	$5.84 \cdot 10^{-5}$	$3.17 \cdot 10^{-3}$	1.66	0.67	0.51	28
8	$1.84 \cdot 10^{-5}$	$1.59 \cdot 10^{-3}$	1.66	1.00	0.13	28

$\gamma = 1$						
$\ell$	error <sub>2</sub>	error <sub>∞</sub>	order <sub>2</sub>	order <sub>∞</sub>	%nz	CG
1	$3.39 \cdot 10^{-2}$	$4.81 \cdot 10^{-2}$	—	—	52	9
2	$1.27 \cdot 10^{-2}$	$3.12 \cdot 10^{-2}$	1.42	0.62	51	21
3	$4.15 \cdot 10^{-3}$	$1.98 \cdot 10^{-2}$	1.61	0.66	48	37
4	$1.29 \cdot 10^{-3}$	$1.25 \cdot 10^{-2}$	1.69	0.66	39	54
5	$3.97 \cdot 10^{-4}$	$7.90 \cdot 10^{-3}$	1.70	0.66	19	69
6	$1.22 \cdot 10^{-4}$	$4.90 \cdot 10^{-3}$	1.70	0.69	6.7	77
7	$3.79 \cdot 10^{-5}$	$3.04 \cdot 10^{-3}$	1.69	0.69	1.9	79
8	$1.13 \cdot 10^{-5}$	$1.15 \cdot 10^{-3}$	1.75	1.40	0.44	79

TABLE 7. Results for the interpolation of the solution of the Laplace equation on the L-shaped domain using the  $C^0$ -smooth Matérn-1/2 RBF and  $\rho = 2$ ,  $q = 4$  as samplet compression parameters.

resulting point cloud, ensuring a specific cardinality for each set. We start with an initial set of 20 points, and at each subsequent level, the cardinality is increased by a factor of 16. In this study, we present results for both nested and non-nested point sets. For the nested case, the indices of the points are randomly shuffled, and subsamples are obtained by selecting the first  $n$  points, where  $n$  represents the desired cardinality. In contrast, for the non-nested case, each subsample is randomly selected from the entire dataset independently, i.e., without enforcing the inclusion of points from previous levels. Unlike previous tests, this experiment is more general, as the points are not arranged on a uniform grid, they are not necessarily nested, and they are not necessarily quasi-uniform. As test function, we interpolate  $f(\mathbf{x}) = (\sqrt[4]{\|\mathbf{x} - \mathbf{x}_0\|_2} + 10^{-4})^{-1}$ . The point  $\mathbf{x}_0$  is selected near the torch that Lucy holds in her left hand. To optimize performance, we use a relatively small value for the parameter  $\gamma$  and set  $\rho = 3$ ,  $q = 2$ , while the a-posteriori threshold is set to  $10^{-5}$ . These adjustments help decrease both computational time and the number of non-zero entries. However, a very small  $\gamma$  can compromise the precision, while a very large  $\gamma$  increases the number of conjugate gradient iterations, thereby increasing computational time. A good trade-off is given by  $\gamma = 0.2$ . Furthermore, we employed a diagonally preconditioned conjugate gradient method with accuracy  $10^{-6}$  to solve the linear system, which reduces the number of iterations by a factor of about three compared to the unpreconditioned case. The number of points per level and the corresponding fill-distances are provided in Table 8.

The error is evaluated on a finer set of 2 000 000 points, which are randomly selected once from the original dataset. The evaluation set remains fixed throughout all experiments to ensure consistency in error measurement. The results using the Matérn-1/2 and Matérn-3/2 RBFs are shown in Tables 9 and 10, respectively.

We observe that the  $C^0$ -smooth Matérn-1/2 RBF performs better in this scenario, primarily due to the improved conditioning of the associated generalized Vandermonde matrix. In both cases, the approximation error is higher than the compression error  $\kappa = 10^{-5}$ .

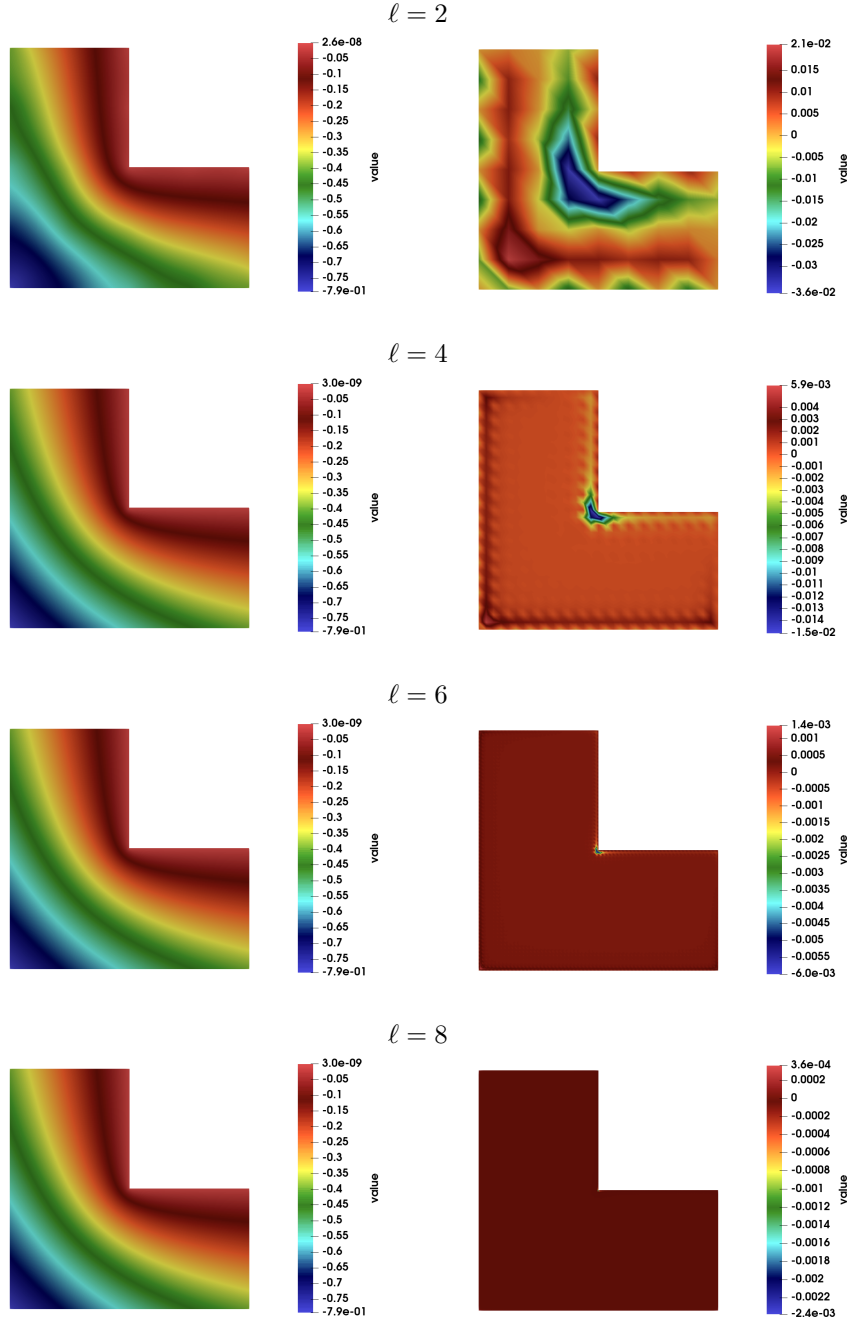


FIGURE 4. Solution (left) and corresponding residuals (right) for the interpolation of the solution to the Laplace equation on the L-shaped domain for levels  $\ell = 2, 4, 6, 8$ .

A visualization of the solution on all five levels  $\ell = 1, \dots, 5$  using the Matérn-1/2 RBF and non-nested points is depicted in Figure 5.

## 8. CONCLUSION

We have proposed an efficient multiscale approach for scattered data interpolation with globally supported RBFs in combination with the samplelet matrix compression. In particular, we have

$\ell$	$N_\ell$	$h$ (nested)	$h$ (non-nested)
1	20	0.25	0.34
2	320	0.15	0.13
3	5 120	0.061	0.064
4	81 920	0.017	0.018
5	1 310 720	0.0051	0.0050

TABLE 8. Number of points per level and corresponding fill-distances for the interpolation on the Lucy point cloud.

$\gamma = 0.2$								
	nested				non-nested			
$\ell$	error <sub>2</sub>	order <sub>2</sub>	%nz	CG	error <sub>2</sub>	order <sub>2</sub>	%nz	CG
1	$5.98 \cdot 10^{-1}$	—	50	8	$4.49 \cdot 10^{-1}$	—	50	9
2	$1.60 \cdot 10^{-1}$	2.58	44	26	$1.27 \cdot 10^{-1}$	1.31	42	28
3	$3.08 \cdot 10^{-2}$	1.83	6.5	49	$2.25 \cdot 10^{-2}$	2.44	6.9	45
4	$5.22 \cdot 10^{-3}$	1.39	0.51	56	$2.36 \cdot 10^{-3}$	1.78	0.50	65
5	$7.94 \cdot 10^{-4}$	1.56	0.03	57	$2.51 \cdot 10^{-4}$	1.74	0.03	69

TABLE 9. Results for the interpolation of a test function on the Lucy point cloud for the  $C^0$ -smooth Matérn-1/2 RBF using  $\rho = 3$ ,  $q = 2$  as samplet compression parameters.

$\gamma = 0.2$								
	nested				non-nested			
$\ell$	error <sub>2</sub>	order <sub>2</sub>	%nz	CG	error <sub>2</sub>	order <sub>2</sub>	%nz	CG
1	$6.16 \cdot 10^{-1}$	—	50	11	$4.50 \cdot 10^{-1}$	—	50	12
2	$1.48 \cdot 10^{-1}$	2.79	45	74	$1.14 \cdot 10^{-1}$	1.43	44	79
3	$2.92 \cdot 10^{-2}$	1.80	6.5	214	$1.73 \cdot 10^{-2}$	2.66	7.0	247
4	$5.41 \cdot 10^{-3}$	1.32	0.51	341	$1.32 \cdot 10^{-3}$	2.03	0.51	398
5	$8.57 \cdot 10^{-4}$	1.53	0.03	349	$1.61 \cdot 10^{-4}$	1.64	0.03	430

TABLE 10. Results for the interpolation of a test function on the Lucy point cloud for the  $C^1$ -smooth Matérn-3/2 RBF using  $\rho = 3$ ,  $q = 2$  as samplet compression parameters.

extended existing results on the boundedness of the condition numbers of the generalized Vandermonde matrices within the multiscale approximation towards globally supported RBFs. For appropriately chosen lengthscale parameters, the condition numbers of the diagonal blocks of the multiscale system stay bounded independently of the level. As a consequence, the diagonally scaled multiscale system becomes well conditioned. We have exploit this fact and derived a general error estimate bounding the consistency error issuing from a numerical approximation of the multiscale system. This result particularly allows to rigorously bound the consistency error arising from the samplet matrix compression. The sparse representation of the multiscale system in samplet coordinates allows for an efficient solution of the linear system by the conjugate gradient method with a bounded number of iterations for a given accuracy, due to the well conditioning. The resulting algorithm has an overall cost of  $\mathcal{O}(N \log^2 N)$  for  $N$  quasi-uniform data sites, given local approximation spaces with exponentially decreasing dimension with decreasing level. The numerical results demonstrate that the presented approach achieves a similar accuracy to the multiscale approach using compactly supported RBFs, as presented in [29], where the corresponding experiments can

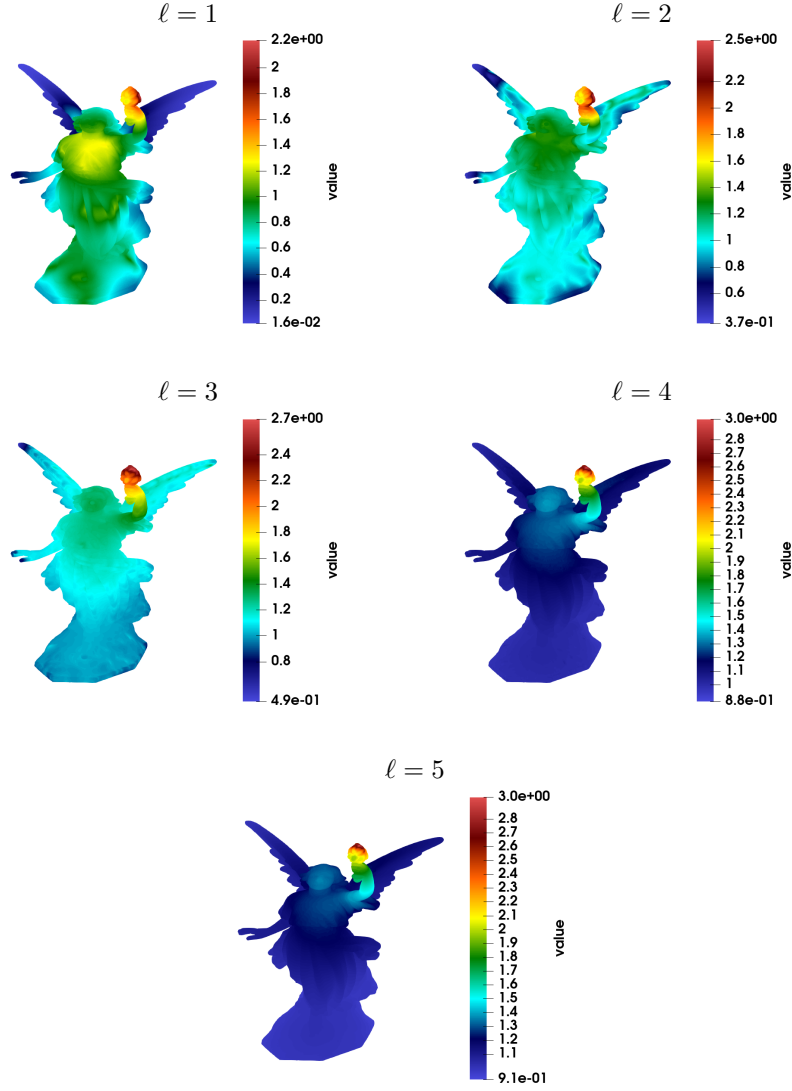


FIGURE 5. Interpolant of the test function on the Lucy point cloud for levels  $\ell = 1, \dots, 5$  using the Matérn-1/2 RBF.

be found. Meanwhile, our approach overcomes previous limitations that made the use of globally supported RBFs impractical for large-scale problems. We have demonstrated that the present multiscale approach can handle datasets with millions of data in both two and three spatial dimensions. As test cases, we have considered smooth and non-smooth data in two dimensions and a complex geometry in three spatial dimensions. In all cases, we achieved accurate results that would have been computationally infeasible without the sample matrix compression.

#### REFERENCES

- [1] D. Alm, H. Harbrecht, and U. Krämer. The  $\mathcal{H}^2$ -wavelet method. *J. Comput. Appl. Math.*, 267:131–159, 2014.
- [2] D. Baroli, H. Harbrecht, and Multerer. Samplet basis pursuit: Multiresolution scattered data approximation with sparsity constraints. *IEEE Trans. Sign. Proc.*, 72:1813–1823, 2024.
- [3] B. Bohn, C. Rieger, and M. Griebel. A representer theorem for deep kernel learning. *J. Mach. Learn. Res.*, 20:Paper No. 64, 32, 2019.
- [4] M. S. Floater and A. Iske. Multistep scattered data interpolation using compactly supported radial basis functions. *J. Comput. Appl. Math.*, 73(1-2):65–78, 1996.
- [5] R. Franke. Scattered data interpolation: tests of some methods. *Math. Comp.*, 38(157):181–200, 1982.

- [6] S. J. Hales and J. Levesley. Error estimates for multilevel approximation using polyharmonic splines. *Numer. Algorithms*, 30(1):1–10, 2002.
- [7] T. Hangelbroek and C. Rieger. Kernel multigrid on manifolds. *J. Complexity*, 86:Paper No. 101900, 26, 2025.
- [8] H. Harbrecht, U. Kähler, and R. Schneider. Wavelet Galerkin BEM on unstructured meshes. *Comput. Vis. Sci.*, 8(3-4):189–199, 2005.
- [9] H. Harbrecht and M. Multerer. Samplers: Construction and scattered data compression. *J. Comput. Phys.*, 471:111616, 2022.
- [10] H. Harbrecht, M. Multerer, and J. Quizi. The dimension weighted fast multipole method for scattered data approximation. 2024.
- [11] H. Harbrecht, M. Multerer, O. Schenk, and C. Schwab. Multiresolution kernel matrix algebra. *Numer. Math.*, 156(3):1085–1114, 2024.
- [12] N.J. Higham. *Accuracy and Stability of Numerical Algorithms*. Society for Industrial and Applied Mathematics, Philadelphia, 1996.
- [13] A. P. Lawrence, M. E. Nielsen, and B. Fornberg. Node subsampling for multilevel meshfree elliptic PDE solvers. *Comput. Math. Appl.*, 164:79–94, 2024.
- [14] S. Le Borne and M. Wende. Multilevel interpolation of scattered data using  $\mathcal{H}$ -matrices. *Numer. Algorithms*, 85:1175–1193, 2020.
- [15] Q. T. Le Gia, I. H. Sloan, and H. Wendland. Multiscale analysis in Sobolev spaces on the sphere. *SIAM J. Numer. Anal.*, 48(6):2065–2090, 2010.
- [16] W. R. Madych. An estimate for multivariate interpolation. II. *J. Approx. Theory*, 142(2):116–128, 2006.
- [17] W. R. Madych and S. A. Nelson. Multivariate interpolation: A variational theory, 1983.
- [18] W. R. Madych and S. A. Nelson. Multivariate interpolation and conditionally positive definite functions. II. *Math. Comp.*, 54(189):211–230, 1990.
- [19] B. Matérn. *Spatial variation*, volume 36 of *Lecture Notes in Statistics*. Springer, Berlin, second edition, 1986.
- [20] C. A. Micchelli. *Interpolation of scattered data: distance matrices and conditionally positive definite functions*, volume 136 of *NATO Adv. Sci. Inst. Ser. C: Math. Phys. Sci.* Reidel, Dordrecht, 1984.
- [21] F. J. Narcowich, R. Schaback, and J. D. Ward. Multilevel interpolation and approximation. *Appl. Comput. Harmon. Anal.*, 7(3):243–261, 1999.
- [22] F. J. Narcowich, N. Sivakumar, and J. D. Ward. On condition numbers associated with radial-function interpolation. *J. Math. Anal. Appl.*, 186(2):457–485, 1994.
- [23] I. Rebai, Y. BenAyed, and W. Mahdi. Deep multilayer multiple kernel learning. *Neural Comput. Appl.*, 27:2305–2314, 2016.
- [24] R. Schaback. Error estimates and condition numbers for radial basis function interpolation. *Adv. Comput. Math.*, 3(3):251–264, 1995.
- [25] J. Tausch and J. White. Multiscale bases for the sparse representation of boundary integral operators on complex geometry. *SIAM J. Sci. Comput.*, 24(5):1610–1629, 2003.
- [26] A. Townsend and H. Wendland. Multiscale analysis in Sobolev spaces on bounded domains with zero boundary values. *IMA J. Numer. Anal.*, 33(3):1095–1114, 2013.
- [27] H. Wendland. Piecewise polynomial, positive definite and compactly supported radial functions of minimal degree. *Adv. Comput. Math.*, 4(4):389–396, 1995.
- [28] H. Wendland. *Scattered data approximation*, volume 17 of *Cambridge Monographs on Applied and Computational Mathematics*. Cambridge University Press, Cambridge, 2005.
- [29] H. Wendland. Multiscale analysis in Sobolev spaces on bounded domains. *Numer. Math.*, 116:493–517, 2010.
- [30] H. Wendland. Multiscale radial basis functions. In *Frames and other bases in abstract and function spaces*, Appl. Numer. Harmon. Anal., pages 265–299. Birkhäuser/Springer, Cham, 2017.
- [31] H. Wendland. *Numerical linear algebra: An introduction*. Cambridge Texts in Applied Mathematics. Cambridge University Press, Cambridge, 2017.
- [32] T. Wenzel, F. Marchetti, and E. Perracchione. Data-driven kernel designs for optimized greedy schemes: a machine learning perspective. *SIAM J. Sci. Comput.*, 46(1):C101–C126, 2024.
- [33] T. Wenzel, G. Santin, and B. Haasdonk. Analysis of target data-dependent greedy kernel algorithms: Convergence rates for  $f$ -,  $f$ - $P$ - and  $f/P$ -greedy. *Constr. Approx.*, 57(1):45–74, 2023.
- [34] A. G. Wilson, Z. Hu, R. Salakhutdinov, and E. P. Xing. Deep kernel learning. In *Artificial intelligence and statistics*, pages 370–378. PMLR, 2016.
- [35] G. B. Wright, A. Jones, and V. Shankar. MGM: a meshfree geometric multilevel method for systems arising from elliptic equations on point cloud surfaces. *SIAM J. Sci. Comput.*, 45(2):A312–A337, 2023.
- [36] Z. Wu. Compactly supported positive definite radial functions. *Adv. Comput. Math.*, 4(3):283–292, 1995.
- [37] Z. Wu and R. Schaback. Local error estimates for radial basis function interpolation of scattered data. *IMA J. Numer. Anal.*, 13(1):13–27, 1993.

SARA AVESANI, ISTITUTO EULERO, USI LUGANO, VIA LA SANTA 1, 6962 LUGANO, SVIZZERA.

*Email address:* `sara.avesani@usi.ch`

RÜDIGER KEMPF, APPLIED AND NUMERICAL ANALYSIS, DEPARTMENT OF MATHEMATICS, UNIVERSITY OF BAYREUTH, 95440 BAYREUTH, GERMANY

*Email address:* `ruediger.kempf@uni-bayreuth.de`

MICHAEL MULTERER, ISTITUTO EULERO, USI LUGANO, VIA LA SANTA 1, 6962 LUGANO, SVIZZERA.

*Email address:* `michael.multerer@usi.ch`

HOLGER WENDLAND, APPLIED AND NUMERICAL ANALYSIS, DEPARTMENT OF MATHEMATICS, UNIVERSITY OF BAYREUTH, 95440 BAYREUTH, GERMANY

*Email address:* `holger.wendland@uni-bayreuth.de`